American Mineralogist, Volume 75, pages 443–463, 1990

The ionic model: Perceptions and realities in mineralogy*

CHARLES W. BURNHAM
Department of Earth and Planetary Sciences, Harvard University, Cambridge, Massachusetts 02138, U.S.A.

ABSTRACT

The ionic model for crystals was devised shortly after the first crystal structures were determined in the early part of this century, but its use was hindered by the difficulty of calculating Coulomb electrostatic sums, and its applicability was diminished by the fact that empirical short-range repulsive potentials could be obtained only for the simplest of structures. Over the past two decades these disadvantages have been overcome, by development of techniques for fitting short-range potentials empirically to data for any structure, and by the important innovation of the modified electron-gas (MEG) formalism by which short-range potentials for closed-shell ions can be determined nonempirically from electron densities. Both techniques have now been employed to examine minimum-energy structures and properties of a variety of mineral systems. In a review of studies of TiO_2 polymorphs, $MgSiO_3$ perovskite, forsterite and its high-pressure polymorphs, quartz, diopside, and albite, the modern applicability of the ionic model to examination of the structures and properties of silicates and oxides is explored. The potential of these methods to contribute significantly to quantitative understanding of crystal-chemical and thermodynamic properties of a wide spectrum of minerals is firmly established.

INTRODUCTION

The ionic model in its simplest form asserts that atoms in a crystal are ionized, with valence electrons transferred from cations to anions. The nearest neighbors of positively charged cations are negatively charged anions and vice versa. The major forces bonding the ions are electrostatic, obeying Coulomb's law for the force between point charges. At short separations the ions are held apart by repulsive forces between partially overlapping electron densities. These ideas led years ago to the important notion that geometrical constraints of packing are a primary factor controlling the structures of ionic solids.

There is a common perception among mineralogists that the ionic model is now outmoded, that it is too simplified, and that because bonding in minerals is rarely purely ionic, the oversimplified model cannot possibly be appropriate. But in reality there exists an undeniable, expanding body of knowledge about mineral behavior acquired using the assumptions of the ionic model. My objective here is to outline some recent advances made using ionic models. By illustrating the kinds of things that can be learned, I hope to show that the ionic model remains an important tool for mineralogists, crystal chemists, and even mineral physicists.

* Adapted from the Presidential Address given at the annual meeting of the Mineralogical Society of America, November 7, 1989, in St. Louis, Missouri. Figures 7, 9, 10, 11, and 12 originally appeared in *Physics and Chemistry of Minerals* and are reprinted here with the permission of Springer-Verlag.

The ionic model

The ionic structure energy is the energy change when infinitely separated ions are brought to their positions in a crystal. The notion that atoms in a solid are held in equilibrium by an attractive force and a more rapidly changing repelling force was suggested as early as 1785 by Bošković,[1] and Grüneisen and Mie both employed generalized potential expressions of the form (Sherman, 1932)

$$W_{ij} = -\frac{a}{r^m} + \frac{b}{r^n}, \quad a, b > 0; n > m. \tag{1}$$

A quantitative theory for ionic solids was developed between 1918 and 1924 by Madelung, Haber, and espe-

[1] Rudjer J. Bošković, born in Dubrovnik, Yugoslavia, in 1711, published a five-volume work titled *Opera pertinentia ad opticam et astronomiam maxima ex parte nova et omnia hucusque inedita in V tomos distributa* in 1785. Among other things, this work contains a "universal law of forces" among particles of matter, which he developed as an outgrowth of Newton's speculations on the subject. From his analysis of collisions of bodies, he argued that the forces acting on elements of matter were alternately attractive or repulsive, depending on the separation distance, and that at very small distances the repulsive force predominated, becoming infinite at zero separation. Historians believe Bošković's ideas represent the first articulation of what would in the 19th century become the concept of fields. Interestingly, Bošković had earlier (around 1742) developed ideas about mountain building that are the precursors of isostasy and had proposed methods for measuring gravity and the mean density of the earth (Gillespie, 1970).

0003–004X/90/0506–0443$02.00

cially Born. The interionic pair potential, W_{ij} (with units of energy), consists of a Coulomb electrostatic term, derived from the force between nonoverlapping ions considered as point charges, and a short-range term arising from ion overlap that is mainly repulsive. Born and Landé (1918) wrote this potential as

$$W_{ij} = \frac{z_i z_j \epsilon^2}{r_{ij}} + \frac{b_{ij}}{r_{ij}^n}, \tag{2}$$

where z_i and z_j are the valences of the interacting ions, ϵ is the electron charge, r_{ij} is the interionic distance, and b_{ij} and n are constants characteristic of the specific interaction between ions i and j. For known structures, b_{ij} could be determined from the equilibrium condition

$$\frac{dW}{dr} = 0 = -z_i z_j \epsilon^2 r_{ij}^{-2} - n b_{ij} r^{-(n+1)}, \tag{3}$$

from which

$$b_{ij} = -z_i z_j \epsilon^2 r_{ij}^{n-1}/n. \tag{4}$$

The exponent n could be determined for certain simple substances from bulk compressibilities. If the structure is fixed by symmetry, and a change in unit-cell volume is directly related to a change in one unique interionic distance, n can be obtained from d^2W/dr^2. A value for n of 9, based on the compressibilities of alkali halides, was frequently used (Pauling, 1928).

From studies of quantum mechanics it had become clear by the late 1920s that the short-range repulsive potential was more appropriately described by an exponential form rather than by the inverse power form (Pauling, 1927). Born and Mayer (1932) wrote this potential as

$$W_{ij(rep)} = \lambda_{ij} \exp(-r_{ij}/\rho_{ij}), \tag{5}$$

where λ_{ij} and ρ_{ij} are parameters characteristic of the interacting ions i and j. Replacing the short-range term in Equation (2) with that from Equation (5), the interionic potential becomes

$$W_{ij} = \frac{Z_i Z_j \epsilon^2}{r_{ij}} + \lambda_{ij} \exp(-r_{ij}/\rho_{ij}). \tag{6}$$

Under the assumption of pairwise additive behavior, the ionic structure energy can be obtained by summing all interionic potentials:

$$W_{tot} = W_{Cou} + W_{short\ range}$$

$$W_{tot} = \tfrac{1}{2} \sum_{\substack{i \\ i \neq j}} \sum_{j} \frac{Z_i Z_j \epsilon^2}{r_{ij}} + \tfrac{1}{2} \sum_{\substack{i \\ i \neq j}} \sum_{j} \lambda_{ij} \exp(-r_{ij}/\rho_{ij}). \tag{7}$$

The summation of Coulomb electrostatic terms is over all ion pairs in the crystal, whereas the summation of short-range terms is generally not required to go beyond nearest neighbors, or second-nearest neighbors in the case of anion-anion interactions. The factor ½ accounts for the fact that in both summations each interaction is included twice.

There are two significant difficulties with Equation 7 that precluded its early application to any but the simplest structures. First, the Coulomb sum converges very slowly, as can be easily appreciated from the fact that alternating shells of further neighbors have opposite valences. Second, the short-range terms involve parameters λ and ρ (or b and n in the case of the inverse power formulation), which had to be determined empirically. There was no readily understood way to calculate the energy of electron overlap from first principles.

As one way to deal with the first problem, the Coulomb summation was written as

$$W_{Cou} = A z_i z_j \epsilon^2 / r_0, \tag{8}$$

where A is a constant depending only on the structure of the crystal—known as the Madelung constant—and r_0 is the unique, or possibly the smallest, cation-anion distance. Madelung (1918) was the first to calculate such a constant, for the NaCl structure. For structures such as NaCl, CsCl, and ZnS, whose atomic coordinates are fixed by symmetry, the madelung constant, A, is truly constant for the structure type, and the Coulomb term for a specific example requires only the specific valences and r_0 for that example. For a structure type as simple as rutile, however, A is a function of both c/a and the one variable atomic coordinate, x_{oxy}. Thus for complex structures, Equation 8 provides no advantage.

Ewald (1921) devised a method to calculate W_{Cou} involving two rapidly converging sums. One is a direct lattice sum whose convergence is accelerated by inclusion of a modification function (complement of the error function) that decreases from 1 to 0 as r_{ij} increases. The error introduced by this modification function is exactly compensated by the second sum, whose convergence is also accelerated by a modification function that decreases from 1 to 0 as $|\mathbf{h}|$ increases, where $\mathbf{h}$ is a reciprocal lattice vector. Bertaut (1952) modified Ewald's method to sum completely in reciprocal space. Both methods derive from the fact that, using the identity

$$1/r = \int_0^\infty e^{-rx}\, dx \qquad (r \neq 0), \tag{9}$$

the Coulomb sums can be replaced by integrals, and by appropriate transformations a Fourier representation of potential can be obtained. Some aspects of the Ewald method are discussed by Nijboer and DeWette (1957), and Burnham (1985) has briefly reviewed the Bertaut method. Both algorithms are widely programmed and give rapid reliable results; examples include WMIN (Busing, 1981), which uses the Ewald method, and ELEN (Ohashi and Burnham, 1972), which uses the Bertaut method.

Energy minimization

With the advent of widely available rapid computing power, determination of minimum-energy structures be-

came a reality. The structure energy of a crystal can be calculated easily using Equation 7, provided appropriate short-range parameters are available. Atomic coordinates and unit-cell dimensions can be varied until the minimum-energy configuration, having $\partial W/\partial x_i = 0$ for all structure parameters x_i, is found. The programs WMIN (Busing, 1981) and METAPOCS (Parker, 1983) are examples that provide this capability. Such energy minimizations yield static structures, strictly speaking, appropriate for P = 0 and T = 0.

As a simple example, Figure 1 is a plot of the net structure energy for MgO, as the difference between the negative Coulomb electrostatic energy and the positive, repulsive, short-range energy, as a function of Mg-O interatomic distance. MgO has the cubic NaCl structure, in which the atoms are fixed by symmetry, all Mg-O distances are identical, and $V_{cell} = (2r_{Mg\text{-}O})^3$. Whereas the minimum appears ill defined at large energy scales, the inset shows clearly at a magnified scale a well defined, almost parabolic, energy minimum. The inset indicates the observed distance, 2.105 Å, as well as several other recently determined minimum-energy distances. The variation in calculated minimum-energy configurations reflects differences in short-range parameters.

To account for the effect of pressure, an additional term, $p\Delta V$, where ΔV is the volume change on compression, is included in the energy minimization. With minimizations carried out at several pressures, the isothermal compressibility and its inverse, the 0 K bulk modulus K_0, can be determined from

$$\frac{1}{K_0} = -\frac{1}{V}\left\{\frac{\partial V}{\partial p}\right\}_T. \qquad (10)$$

It should be noted that the calculated bulk modulus depends essentially on the second derivatives of the pair potentials. Specific normal or shear stresses may be applied as well, and the calculated strains in the resulting model are used to obtain elastic moduli (Busing and Matsui, 1984).

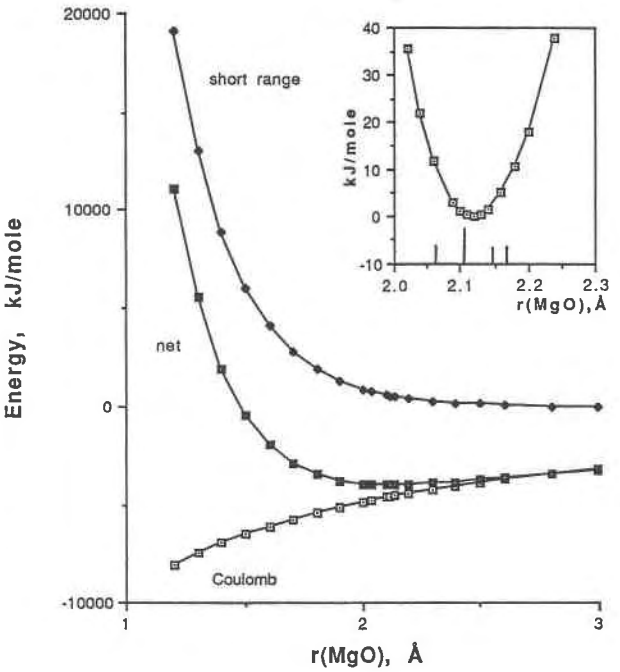

Fig. 1. Periclase structure energy as a function of Mg-O separation. Coulomb term obtained from Equation 8 using A = 1.747566 for the NaCl structure; MEG short-range term obtained using λ and ρ from linear regressions (Table 1) extrapolated to oxygen shell radius of 1.205 Å. Inset shows net structure energy, relative to zero at 2.12 Å minimum, in the region close to the minimum; short vertical bars indicate other reported MEG-determined minima (Tossell, 1980; Muhlhausen and Gordon, 1981a; Hemley et al., 1985; Mehl et al., 1986); longer vertical bar indicates observed Mg-O distance, 2.105 Å (Hazen, 1976a).

Calculation of thermodynamic properties

Further development of thermodynamic properties of ionic crystals from the simple pair potential model embodied in Equations 6 and 7 requires lattice dynamical calculations. The complete internal energy, E, consists of the static structure energy, W, plus the vibrational energy, written as a sum over normal vibrational modes (Born and Huang, 1954)

$$E = W + \tfrac{1}{2}\sum_i \hbar\omega_i + \sum_i \frac{\hbar\omega_i}{\exp(\hbar\omega_i/kT) - 1} \qquad (11)$$

where the ω_i are frequencies of normal vibration modes, $\hbar$ is Planck's constant, k is the Boltzmann constant, and T is temperature in K. The vibrational energy can be recast in terms of an integral over frequency (e.g., Price et al., 1987b)

$$E = W + \int_0^{\omega_m} \hbar\omega \{\tfrac{1}{2} + [\exp(\hbar\omega/kT) - 1]^{-1}\} G(\omega)\, d\omega. \qquad (12)$$

Here ω_m is the maximum vibrational frequency of the crystal and $G(\omega)$ is the density-of-states function, such that $G(\omega)\, d\omega$ is the number of normal modes in the first Brillouin zone having frequencies between ω and $\omega + d\omega$. At 0 K, the vibrational contribution to internal energy is from zero-point energy alone, $\frac{1}{2}\Sigma\hbar\omega_i$.

The relationship between interionic potentials (Eq. 6) and the frequencies of normal vibration modes is embodied in Newtonian equations of motion, and is discussed in several crystal physics texts (e.g., Born and Huang, 1954; Cochran, 1973). Price et al. (1987a) effectively review the path from the fundamental notion that the restoring force encountered by an ion i displaced by a small vector $\mathbf{u}_i$ from its equilibrium position is given by

$$F_i = \partial W/\partial \mathbf{u}_i \qquad (13)$$

to the resulting 3n equations of motion

$$m\omega^2(\mathbf{k})\mathbf{e}(\mathbf{k}) = \mathrm{D}(\mathbf{k})\mathbf{e}(\mathbf{k}), \tag{14}$$

where n is the number of atoms in the unit cell, m is atom mass, $\mathbf{k}$ is the wave vector of the vibration (whose values range just through the first Brillouin zone of the crystal), $\mathbf{e}(\mathbf{k})$ is the polarization vector describing the atomic displacements for a particular vibration, and $\mathrm{D}(\mathbf{k})$ is the dynamical matrix

$$\mathrm{D}(\mathbf{k}) = \sum_{ij} \frac{\partial^2 W}{\partial \mathbf{u}_i \partial \mathbf{u}_j} \exp(i\mathbf{k}\cdot\mathbf{r}_{ij}). \tag{15}$$

For a given value of $\mathbf{k}$, solution of Equation 14 yields 3n eigenvalues, each of which corresponds to the squared frequency, $\omega^2(\mathbf{k})$, of a normal vibration mode. The associated eigenvectors, $\mathbf{e}(\mathbf{k})$, describe the atomic displacements associated with each mode. It is important to note that calculated vibration frequencies depend on second derivatives of pair potentials. Eigenvalues calculated for $\mathbf{k} = 0$, the long wavelength limit, correspond to frequencies measured by infrared and Raman spectroscopy, thus providing for comparisons with experimental data. As will be shown later, extensive calculations at numerous values of $\mathbf{k}$ throughout the first Brillouin zone are required to evaluate the phonon-dispersion relations and to calculate a density-of-states function, $G(\omega)$, which is needed to evaluate the total vibration energy using Equation 12.

Calculations of thermal properties and equations of state require, in addition to the density-of-states function, $G(\omega)$, knowledge of the mode Grüneisen parameters, γ_i, given by (Born and Huang, 1954),

$$\gamma_i = \frac{\mathrm{d}\ln(\omega_i)}{\mathrm{d}\ln(V)}. \tag{16}$$

From the constant volume heat capacity, C_V, given by

$$C_V = \left[\frac{\partial E}{\partial T}\right]_V = \mathrm{k}\int_0^{\omega_m} \frac{(\hbar\omega/\mathrm{k}T)^2 \exp(\hbar\omega/\mathrm{k}T)}{[\exp(\hbar\omega/\mathrm{k}T) - 1]^2} G(\omega)\,\mathrm{d}\omega, \tag{17}$$

one obtains the heat capacity at constant pressure, C_p, using

$$C_p = C_V + \beta^2 T V K_T, \tag{18}$$

from which the entropy is obtained using $S = \int (C_p/T)\,\mathrm{d}T$. In Equation 18, K_T is the isothermal bulk modulus and β is the coefficient of volume expansion. Following Price et al. (1987b), β can be determined from

$$\beta = \gamma_{th}(C_V/K_T)V \tag{19}$$

where γ_{th} is the thermal Grüneisen parameter and K_T is determined from elastic constants, assumed to be independent of temperature. The mode Grüneisen parameters, γ_i, determined using Equation 16, represent the variation of vibration frequency with molar volume. Since ω varies with $\mathbf{k}$ according to the dispersion relations, there is an unlimited number of γ_i's. Nevertheless, an average Grüneisen parameter, $\bar{\gamma}$, can be calculated from

$$\bar{\gamma} = \frac{\mathrm{d}\langle\ln(\omega)\rangle}{\mathrm{d}\ln(V)}. \tag{20}$$

Within the framework of the quasiharmonic approximation, which ignores anharmonic vibrational effects and assumes that Equation 13 is exact, it has been shown (Slater, 1939) that the thermal Grüneisen parameter, γ_{th}, is equal to the mean mode Grüneisen parameter, $\bar{\gamma}$.

Assuming that one has appropriate interionic pair potentials (Eq. 6), minimum-energy static structures can be calculated using Equation 7 for any pressure. The substantially more difficult and time consuming quasiharmonic lattice dynamical calculations can then be carried out for several volumes. With strategies based on relationships outlined here, elastic moduli and Grüneisen parameters can be obtained, and from them isothermal compressibilities, coefficients of volume expansion, and heat capacities, leading to determinations of entropy and Gibbs free energy. In theory, then, equations of state of complex ionic crystals and relative stabilities among polymorphs are accessible directly from interionic pair potentials within the framework of the ionic model, using energy minimizations and lattice dynamical calculations.

Short-range potentials

The extent to which simulations of structures and properties can be successful depends largely on the integrity of the short-range potentials. Given that these had to be determined empirically until recently, two questions had to be faced: First, what is the most appropriate parameterization? And next, how will the parameters be determined?

Various modifications of the standard Born-Mayer form (Eq. 5) have been devised. One form, first used by Gilbert (1968), modifies the Born-Mayer parameterization according to

$$W_{ij(rep)} = (\mathrm{B}_i + \mathrm{B}_j)\exp[(\mathrm{A}_i + \mathrm{A}_j - r_{ij})/(\mathrm{B}_i + \mathrm{B}_j)] \tag{21}$$

where, instead of parameters λ and ρ being specific for a given interaction i − j, the potential is written in terms of parameters A_i and B_i that are "properties" of each ion. After As and Bs have been determined by some means for a variety of ions, the potentials for different interactions are then easily formulated.

A number of workers (e.g., Price et al., 1987a) have employed what is sometimes called the Buckingham parameterization, in which an attractive van der Waals term, accounting for instantaneous dipole-dipole interactions, is added to a Born-Mayer form:

$$W_{ij(rep)} = \mathrm{A}_{ij}\exp(-r_{ij}/\mathrm{B}_{ij}) - \mathrm{C}_{ij}/r_{ij}^6. \tag{22}$$

Additional expressions have been employed to account

for certain polarizable ions or for the covalent behavior of, for example, the Si-O bond. A simple shell model for polarizable anions separates the ion into a core containing all the mass surrounded by a shell of charge Y representing the outer valence electrons (Price et al., 1987a). The core and shell are separated by r and are coupled by a harmonic spring with a spring constant, k, leading to the potential $W_{cs} = kr^2$, and polarizability, $\alpha = (Y\epsilon)^2/(k + r)$. To model Si-O, Price and Parker (1984) used a Morse potential whereas Sanders et al. (1984) and Matsui and Busing (1984) employed various kinds of bond-bending potentials.

Having formulated the short-range potential for various interactions, values for the parameters must be found empirically. As mentioned earlier, bulk compressibilities are useful only for the simplest structures in which all interionic separations are determined by the lattice parameters alone. Since $dW/dr_{ij} = 0$ at equilibrium and $d^2W/dr_{ij}^2 = k_{ij}$, where k_{ij} is the force constant for ij stretching, λ_{ij} and ρ_{ij} for the Born-Mayer short-range potential formulation may be determined from fully characterized vibrational spectra (Lasaga, 1980). This procedure requires, however, that simple stretching or bending modes be readily identifiable, which further requires a sometimes unrealistic assumption that the vibrations are suitably localized (McMillan, 1985).

During the past decade a substantial number of ionic modeling studies have used short-range potential parameters determined by fitting to known structures. Both the programs WMIN (Busing, 1981) and METAPOCS (Parker, 1983) are capable of determining a set of short-range parameters that best reproduce one or more known structures, and fittings can be carried out with any of a variety of potential formulations. Recognizing that silicates and many oxides of interest to mineralogists have real electron distributions substantially different from those expected in truly ionic crystals (e.g., Sasaki et al., 1980; Fujino et al., 1981), several workers have carried out fittings using variable ionic charges. I have previously reviewed a number of silicate modeling studies carried out with short-range potentials determined by a variety of empirical fittings to observed structures (Burnham, 1985).

All empirically determined short-range potentials include implicitly the consequences of the details of the bonding in whatever structures are used for fitting, regardless of whether the observations are compressibilities, vibrational force constants, or the structural parameters themselves. Thus ionic modeling with such potentials includes some effects related to lack of pure ionicity. Insofar as these short-range parameters reflect specific bonding circumstances, significant questions arise as to the appropriateness of applying such parameters to the same interactions in other structures. This is the issue of transferability: Will Mg-O short-range potentials determined from properties of periclase, for example, be appropriate when applied to modeling of Mg-O octahedra in, say, olivine? Some examples that I discuss below bear on this important question.

Given that few solids are known to be purely ionic, one might legitimately ask how the ionic model, with a cohesive energy represented by Equation 7, can be expected to yield useful results for any but a small handful of the most ionic phases. Clearly some elaborations of short-range potentials, mentioned above, attempt explicitly to accommodate nonionic effects. But more generally it is worth pointing out that the model, as embodied in Equation 7, is addressed to central forces between atoms, and assumes, with some justification, that the cohesive energy is closely approximated by pairwise addition of these interionic potentials. It does not speak to the reality of valence elctron distributions, but assumes, regardless of these distributions, that the energetics are adequately described. I reemphasize that empirical short-range potentials include implicitly the effects of a particular electron distribution, and to the extent that such distributions differ from structure to structure, the transferability of such potentials will be diminished.

The modified electron-gas (MEG) model

A model for interactions between closed-shell ions with short-range potentials determined nonempirically from electron-gas theory was introduced by Gordon and Kim (1972). The model assumes that the interaction between two closed-shell ions is a function of their electron densities. If ρ_i and ρ_j are two partly overlapping charge densities, the total charge density, ρ_{ij}, is assumed to be simply the sum of the individual charge densities; thus in the overlap region, the densities are assumed to be additive. The interaction energy is given by

$$W = W_{Cou} + W_{sr} + W_{se}, \tag{23}$$

where W_{Cou} is a Coulomb interaction, W_{sr} is the short-range energy, and W_{se} is ion self-energy. Charge densities, ρ_i, for closed-shell ions are obtained from Hartree-Fock self-consistent field calculations using Slater or other analytic extended-basis sets. Although from the perspectives of mineralogists and crystals chemists, calculations using this model might easily be termed ab initio because no empirical parameters are used, a more rigorous view holds that the model should not carry that label because the charge densities, once calculated, are not varied, and interaction energies are derived from these fixed, assumed additive, densities.

W_{Cou} is calculated directly as in the standard ionic model for point charges. It is applicable to the nonoverlapped portion of the ion electron densities. There is a much smaller nonpoint Coulomb contribution, arising within the overlapped portion of the charge densities, that is calculated exactly and included as part of W_{sr}.

The short-range energy, W_{sr}, is calculated using energy-density functionals obtained from electron-gas theory (Gordon and Kim, 1972; Waldman and Gordon, 1979). Separate functionals are employed for three components of the short-range energy, namely kinetic, exchange, and correlation energies:

$$W_{sr} = \int d^3r[\rho_{ij}E_G(\rho_{ij}) - \rho_i E_G(\rho_i) - \rho_j E_G(\rho_j)] \quad (24)$$

and

$$E_G(\rho) = E_{kin} + E_{exch} + E_{corr}. \quad (25)$$

The energy-density functionals (Muhlhausen and Gordon, 1981a) are shown at bottom of page.

C_k, C_x, and C_c are density-functional correction factors, introduced by Waldman and Gordon (1979), that modify the original electron-gas theory. The purpose of the correction factors is to compensate, without disrupting the simplicity of the electron-gas formalism, for known errors arising from gradients in nonuniform densities (Gordon and Kim, 1972) that lead to significant errors in the predicted potential-well depths of rare-gas systems. Correction factors are given by Waldman and Gordon (1979) for various rare-gas interactions; these are appropriate for corresponding isoelectronic ion-ion corrections.

The kinetic and exchange functionals are known exactly, but the correlation functional is more complicated. Indeed, alternatives to the Gordon and Kim (1972) interpolation formula (Eq. 26c) have been suggested; Clugston (1978) has discussed these in the context of an overall assessment of the electron-gas model.

The fundamental assumption of MEG theory is that the total charge density of ions in a crystal is appropriately considered to be the superposition of charge densities of separated ions. It assumes, like earlier ionic models, that the net interaction energy is suitably represented by a pairwise additive approximation. Many-body contributions that arise as ions are juxtaposed in a crystal may add nonlinearities to the density functionals for short-range energy terms, and they may, additionally, cause changes in the free-ion charge densities. These changes can be divided into two categories: (1) ion size changes that retain spherical symmetry, and (2) anisotropic distortions of charge density owing to field gradients in the crystal that lead to dipolar or higher-order multipolar interactions. Muhlhausen and Gordon (1981a) demonstrated that, whereas nonlinear many-body effects are of little significance, isotropic-size changes owing to the effects of potentials on ions in a crystal are important. Following the strategies of Pachalis and Weiss (1969) and Watson (1958), they calculate a "stabilized" ion charge density by surrounding the ion with a spherical shell having radius r_0 and charge Q (= $-z$) at its surface. The shell potential, V_{sh}, is:

$$V_{sh}(r) = \begin{cases} Q/r_0 & \text{for } r \le r_0 \\ Q/r & \text{for } r > r_0. \end{cases} \quad (27)$$

Thus the shell potential seen by the ion can be adjusted by changing the shell radius, r_0. Since this shell potential mimics the crystal field seen by the ion, Muhlhausen and Gordon (1981a) argue that the most appropriate shell radius is one that yields a shell potential equal to the Madelung (Coulomb) potential at the ion site. The shell potential effectively alters the size of the ion, which changes the charge density and hence the short-range interactions with adjacent ions. Muhlhausen and Gordon (1981a) show that these effects are much more pronounced for anions than cations, and, indeed, that shell stabilization is not needed for cations. The ion self-energies, W_{se} in Equation 23, correspond to the energy differences between free ions and shell-stabilized ions and are an important part of the total energy. For O, because the isolated divalent anion does not exist stably, the self-energy includes, in addition, the energy for the reaction $O^{2-} \rightarrow O^{1-} + e^-$.

Parameterization of MEG short-range potentials

Energy minimizations using MEG theory with shell-stabilized anion charge densities requires that short-range potentials be calculated for a variety of anion shell radii covering the range of anion site potentials anticipated. In addition, the anion self-energies must be calculated as a function of shell radius. As minimization proceeds, anion site potentials may change; in response, cation-anion and anion-anion short-range pair potentials calculated with new anion shell radii must be used, and total energies will change slightly as new anion self-energies are used. Final energy minimization must demonstrate self-consistency, that is that short-range energies are consistent with anion shell radii whose stabilizing potentials agree with anion site potentials. Muhlhausen and Gordon (1981a), Hemley and Gordon (1985), and others calculate short-range energies for each kind of interaction for a range of shell-stabilized anion wave functions over a range of ion separations. The short-range energy for a pair interaction at a specific separation is obtained by interpolation.

Post and Burnham (1986a) have fitted MEG-calculated short-range energies to the Born-Mayer exponential form

---

$$E_{kin} = (3/10)(3\pi^2)^{2/3}\, C_k \rho^{2/3} \quad (26a)$$

$$E_{exch} = -(3/4)(3/\pi)^{1/3}\, C_x \rho^{1/3} \quad (26b)$$

$$E_{corr} = \begin{cases} C_c(-0.438 r_s^{-1} + 1.325 r_s^{-3/2} - 1.47 r_s^{-2} - 0.4 r_s^{-5/2}) & \text{for } r_s \ge 10 \\ C_c(0.01898 \ln(r_s) - 0.06156) & \text{for } 0.7 \le r_s \le 10 \\ C_c(0.0311 \ln(r_s) - 0.048 + 0.009 r_s \ln(r_s) - 0.01 r_s) & \text{for } r_s \le 0.7 \end{cases} \quad (26c)$$

where $r_s = (3/4\pi\rho)^{1/3}$.

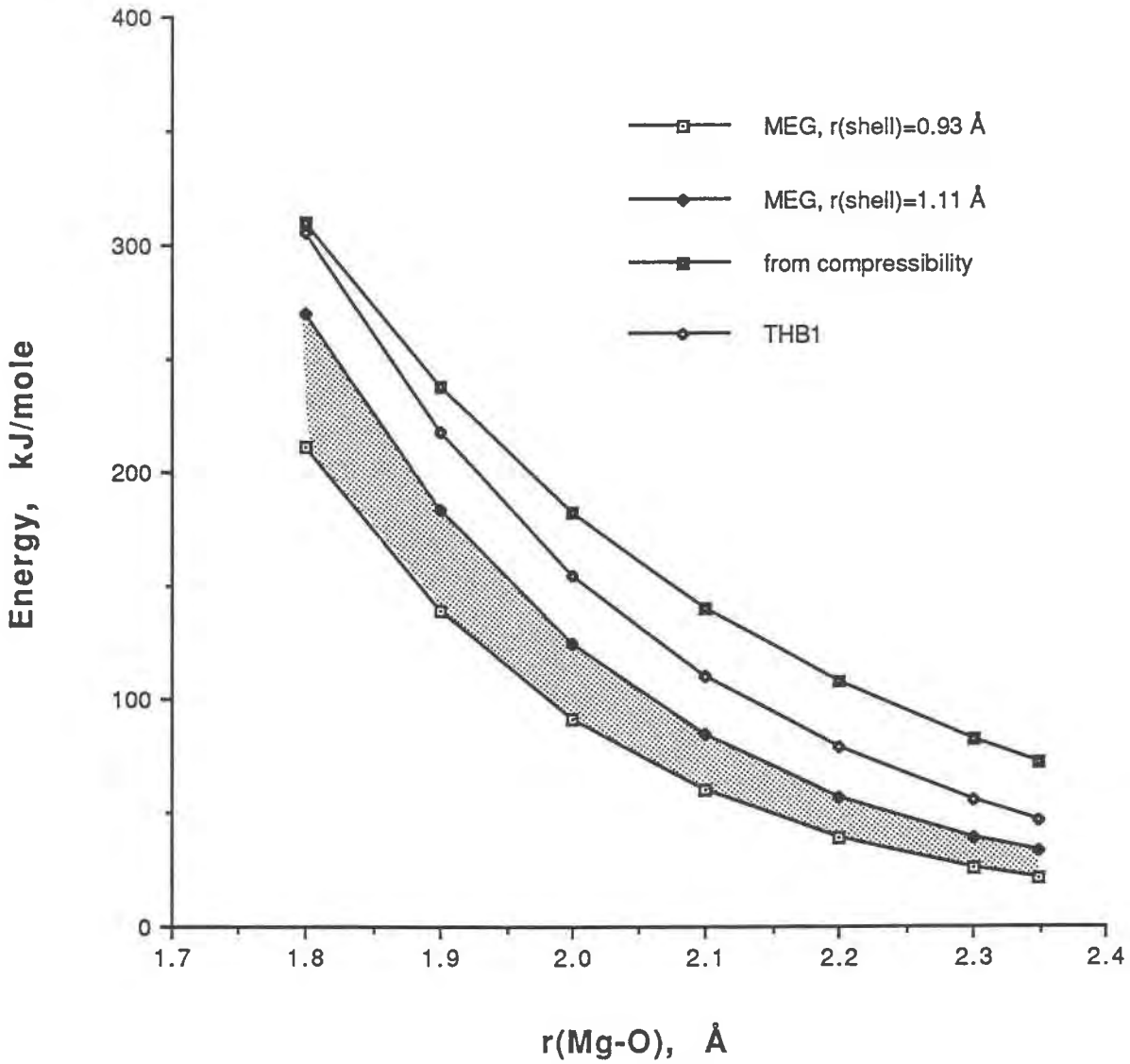

Fig. 2. Mg-O short-range potentials as a function of Mg-O separation. Shaded region is bounded by MEG potentials for oxygen shell radius of 0.93 Å (lower curve) and for oxygen shell radius of 1.11 Å (upper curve). Other curves are obtained from the empirical THB1 potential (Price et al., 1987a; Lewis, 1985) and from periclase compressibility (Ohashi and Burnham, 1972).

(Eq. 5). For a given ion pair and specific anion shell radius, the least-squares values for λ_{ij} and ρ_{ij} reproduce well the MEG short-range energies over the full range of expected nearest neighbor distances, or next-nearest neighbor distances in the case of anion-anion interactions; correlation coefficients exceed 0.9995 in all cases. Examination of the energy-density functionals (Eq. 26) shows that whereas the kinetic energy term is repulsive, both the exchange and correlation terms are attractive. Because kinetic energy and exchange energy are proportional to $\rho^{2/3}$ and $\rho^{1/3}$ respectively, the potential curve will be attractive at large separations. Clearly the Born-Mayer exponential form is inappropriate under those circumstances, but realistic nearest and next-nearest neighbor separations are well within the repulsive regime.

For some ion pairs, Post and Burnham (1986a, Table 1) have determined Born-Mayer parameters, λ and ρ, for several anion shell radii. For Mg-O, λ's and ρ's were determined for six O shell radii from 0.93 Å to 1.11 Å, corresponding to O site potentials ranging from 2.15 to 1.80 ϵ/Å. Figure 2 is a plot of the resulting Mg-O short-range pair potentials for the smallest (0.93 Å) and largest (1.11 Å) O shell radii. As shell radius increases, corresponding to a reduction of site potential (i.e., a lower crystal field at the anion site), the O ion wave functions relax, and for a given Mg-O separation, the repulsive energy increases. As shell radius decreases, repulsion energy at a given separation decreases in response to the contracting anion wave functions. In essence, the anions are no longer rigid, and short-range effects respond to changes

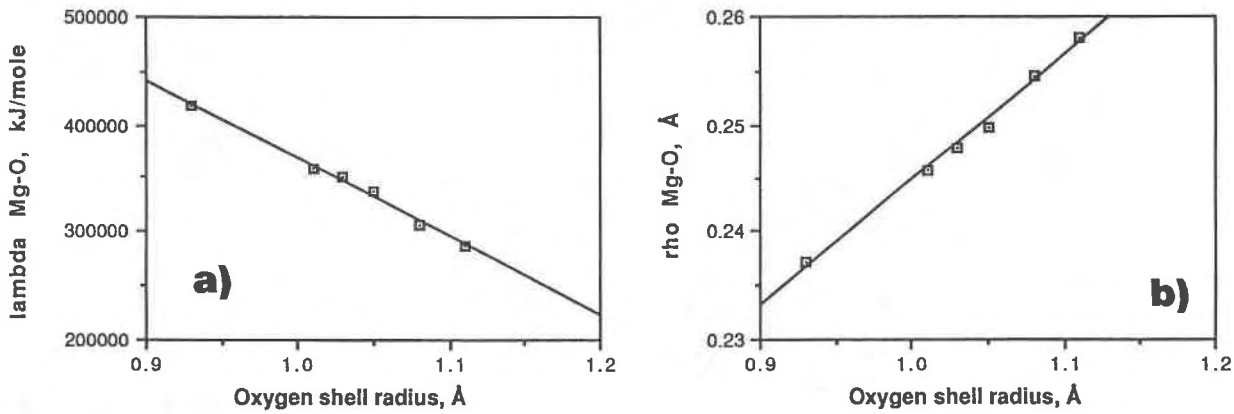

Fig. 3. Born-type MEG-determined short-range potential parameters for Mg-O interactions. (**a**) λ versus oxygen shell radius; (**b**) ρ versus oxygen shell radius. Regression equations given in Table 1.

in crystal field. Figure 2 shows, for comparison, an Mg-O short-range potential determined from compressibility of periclase (Ohashi and Burnham, 1972) and one determined by fitting to the structure and elastic data of MgO (Lewis, 1985); the latter potential was used by Price et al. (1987a, 1987b) to model the Mg_2SiO_4 polymorphs.

Recently we observed, quite by accident, that the variation of λ and ρ with anion shell radius is remarkably linear, at least over the range of shell radii investigated. Table 1 gives linear regression equations for both λ and ρ against shell radius for Mg-O, Si-O, and O-O, which are the only pairs for which Post and Burnham (1986a) gave values for more than three anion shell radii. The linear variations of Mg-O λ and ρ values with O shell radius are shown graphically in Figure 3. Clearly a further systematic compilation and analysis of MEG-derived Born-Mayer short-range parameters is in order, both to examine the extent to which linearity holds and to provide in convenient form theoretical short-range parameters for a large number of useful closed-shell ion pairs.

MEG, SSMEG, and PIB

Following early application of electron-gas theory to ionic solids (Gordon and Kim, 1972), and introduction of the density-functional correction factors (Waldman and Gordon, 1979), the MEG theory has proved increasingly successful at modeling the structures and properties of alkali halides (Cohen and Gordon, 1975), alkaline-earth oxides (Cohen and Gordon, 1976), and a variety of related materials with rather simple structures (Tossell, 1980). Tossell's (1980) calculations on several less ionic oxides appeared to suggest rather significant limitations as ionicity decreases. Significant difficulties with the rigid-ion MEG model were overcome, however, when Muhlhausen and Gordon (1981a, 1981b) introduced anion shell stabilization (SSMEG) as discussed above; they demonstrated that SSMEG represented a first-order improvement because it effectively dealt with the most important many-body crystal field effects. Whereas Post and Burnham (1986a) used SSMEG to model static structures of a variety of minerals, others employed SSMEG in quasiharmonic lattice dynamical calculations to model high temperature and pressure equations of state for alkali halides (Hemley and Gordon, 1985) and MgO (Hemley et al., 1985).

The self-consistency required by SSMEG is achieved by providing to the actual energy minimization short-range cation-anion and anion-anion interactions calculated separately using shell-stabilized anion wave functions appropriate for the observed site potentials. Appropriate anion self-energies are added separately after energy minimization. Clearly a more desirable procedure would be to incorporate the dependence of short-range potential and of anion self-energy on anion site potential directly in the energy minimization. This has been done by Boyer et al. (1985), who term the improved procedure the potential-induced-breathing model, PIB, after the notion that anion wave functions respond dynamically during min-

Table 1. Linear regression equations for short-range energy parameters

Ion pair	Linear regression	Correlation coefficient	Shell radius range (Å)	Ion separation range (Å)
Mg-O	$\lambda = 1.0958 \times 10^6 - 7.2747 \times 10^5 (r_{shell})$	0.992	0.93–1.11	1.80–2.35
	$\rho = 0.1282 + 0.1166 (r_{shell})$	0.997		
Si-O	$\lambda = 9.4285 \times 10^5 - 5.7807 \times 10^5 (r_{shell})$	0.999	0.93–1.11	1.48–1.80
	$\rho = 0.1285 + 0.1135 (r_{shell})$	0.999		
O-O*	$\lambda = 1.4852 \times 10^6 - 1.1824 \times 10^6 (r_{shell})$	0.993	0.93–1.11	2.38–2.91
	$\rho = 0.1001 + 0.1877 (r_{shell})$	0.992		

Note: λ in kJ/mol; ρ in Å.
* For identical shell radii on both anions only.

TABLE 2. MEG-based minimum energy structures of rutile and anatase compared with observed structures (after Post and Burnham, 1986a)

	Rutile ($P4_2/mnm$)		Anatase ($I4_1/amd$)	
	Observed	Minimum energy*	Observed	Minimum energy*
Unit cell				
a (Å)	4.594	4.491 (−2.2)	3.776	3.689 (−2.3)
c	2.958	3.063 (+3.5)	9.486	10.067 (+6.1)
V (Å^3)	62.43	61.78 (−1.0)	135.25	137.00 (+1.3)
Interatomic distances				
Ti-O (×4) (Å)	1.948	1.961 (+0.7)	1.930	1.909 (−1.1)
Ti-O (×2)	1.980	1.935 (−2.3)	1.973	2.030 (+2.9)
⟨Ti-O⟩	1.959	1.952 (−0.4)	1.944	1.949 (+0.3)
O-O (sh)	2.536	2.462 (−2.9)	2.459	2.405 (−2.2)
O^{2-} shell radius (Å):		1.11		1.08

* Values in parentheses are % deviations from observed.

imization to changes of site potential. In studies of alkaline earth oxides (Mehl et al., 1986) and rutile and stishovite (Cohen et al., 1987), the PIB model has been shown to provide a significantly improved capability to simulate dynamical and elastic properties. In particular, it reproduces observed violations in cubic structures of the Cauchy condition of elasticity, $c_{12} = c_{44}$, which rigid-ion models cannot do.

Modeling results

To illustrate the strengths of the ionic model, as well as some of its weaknesses, I now examine several applications to minerals with nontrivial structures. These examples test the model rather severely, from its ability to predict equations of state at high temperatures and pressures to its ability to reproduce complex low-symmetry structures and their response to mineralogically important phenomena such as order-disorder.

TiO_2 polymorphs

Post and Burnham (1986a) used SSMEG to model the static structures of rutile, anatase, and brookite and to determine their relative energies. Tables 2 and 3 compare unit-cell dimensions and interatomic distances of the model structures with observation. Energy minimizations were carried out within the constraints of the observed space groups, although it certainly would have been possible to test structural stability against reduced symmetry, of course at the expense of substantially increased computer time. For both rutile and anatase, the unit-cell volumes are matched to about 1%, whereas a axes are short by 2% and c axes are long, by 3½% in rutile and 6% in anatase. In both observed structures the Ti octahedra have at least symmetry 4, with two axial Ti-O distances different from four equatorial distances. The rutile model reproduces the magnitude of the distortion well, but in the wrong sense, whereas the anatase model magnifies the observed distortion by about three times; mean Ti-O distances are modeled very well. Calculated shared O-O edges are short by 2–3%. Note that O shell radii are different in the two structures, reflecting different O site potentials. The orthorhombic brookite structure is modeled well: Cell edges match to within 1.5%, cell volume matches almost exactly, and individual Ti-O distances reflect a well-matched distortion of the Ti octahedron. Two distinct O-O shared edges are again calculated short by 2%.

Figure 4 compares the calculated cohesive energies of the minimum-energy model structures and the observed structures. Relative energies calculated without the anion self-energies are incorrect, showing anatase more stable than rutile; but when the appropriate self-energies are included, the relative stabilities become correct. The calculated ΔW between rutile and anatase—0.9 kcal/mol for the observed structures and 0.1 kcal/mol for the calculated structures—compares well with the calorimetrically obtained value of −1.3 kcal/mol for ΔH_{298} for anatase → rutile (Navrotsky and Kleppa, 1967). Although it has been suggested that the relative stabilities of the three polymorphs might reflect the number of shared edges per octahedron (Evans, 1966), the calculations show that brookite, with three shared edges, is less stable than either anatase, with four, or rutile, with two. This sequence

TABLE 3. MEG-based minimum energy structure of brookite compared with observed structure (after Post and Burnham, 1986a)

	Brookite ($Pcab$)	
	Observed	Minimum energy*
Unit cell		
a (Å)	9.184	9.171 (−0.1)
b	5.447	5.373 (−1.4)
c	5.145	5.224 (+1.5)
V (Å^3)	257.38	257.42 (+0)
Interatomic distances		
Ti-O1 (Å)	1.865	1.904 (+2.1)
Ti-O1′	1.992	1.998 (−0.3)
Ti-O1″	1.994	1.929 (−3.3)
Ti-O2	1.919	1.956 (+1.9)
Ti-O2′	1.946	1.931 (−0.8)
Ti-O2″	2.039	2.017 (−1.1)
⟨Ti-O⟩	1.959	1.956 (−0.4)
O1-O1 (sh)	2.485	2.434 (−2.1)
O2-O2 (sh)	2.514	2.462 (−2.1)

Note: O^{2-} shell radii: O1 = 1.11 Å, O2 = 1.10 Å.
* Values in parentheses are % deviations from observed.

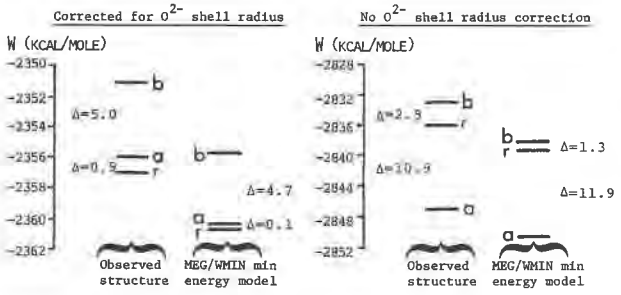

Fig. 4. Calculated structure energies for TiO_2 polymorphs. The letter a = anatase; b = brookite; r = rutile. From Burnham (1985).

matches the observed natural abundances of the three polymorphs.

Cohesive energies are calculated with respect to separated free ions, essentially as a gas phase. If a Born-Haber cycle can be calculated, an observed dissociation energy can be obtained. In the case of rutile the calculated cohesive energy is about 5% greater than that obtained from a Born-Haber calculation. In many applications energy differences between phases are more important than the absolute energy of any individual phase; if the phases under comparison are similar, then these energy differences are undoubtedly better determined than the absolute energies. Since in many cases the vibrational characteristics of structurally similar phases are not markedly different, free-energy differences will consist largely of static cohesive energy differences.

$MgSiO_3$ perovskite

There is a rapidly expanding literature devoted to the likely role of $MgSiO_3$ perovskite in the earth's lower mantle (e.g., Ringwood, 1962; Yagi et al., 1978; Jeanloz and Thompson, 1983). Because it is difficult to conduct experiments under the pressure-temperature conditions found there, a model that is capable of yielding theoretically the equations of state and thermodynamic properties of phases under lower mantle conditions would have wide importance. A variety of empirical short-range potentials, mostly obtained from fits to the observed perovskite structure, were used by Wall et al. (1986) to simulate the cubic, tetragonal, and orthorhombic structures. Rigid-ion MEG methods have been used to simulate the distortions and calculate the lattice dynamics of both $MgSiO_3$ and $CaSiO_3$ (Wolf and Jeanloz, 1985; Wolf and Bukowinski, 1987). SSMEG methods (Hemley et al., 1987), and PIB methods (Cohen, 1987) have proved most successful, however, for calculating structures, equations of state, and dynamical properties of these perovskites.

The structure of ideal cubic perovskite, ABO_3, contains a corner-sharing network of B octahedra with large A cations occupying 12-coordinated sites between octahedra (Fig. 5a). There are several lower-symmetry derivatives of the ideal structure, related to the ideal by relative

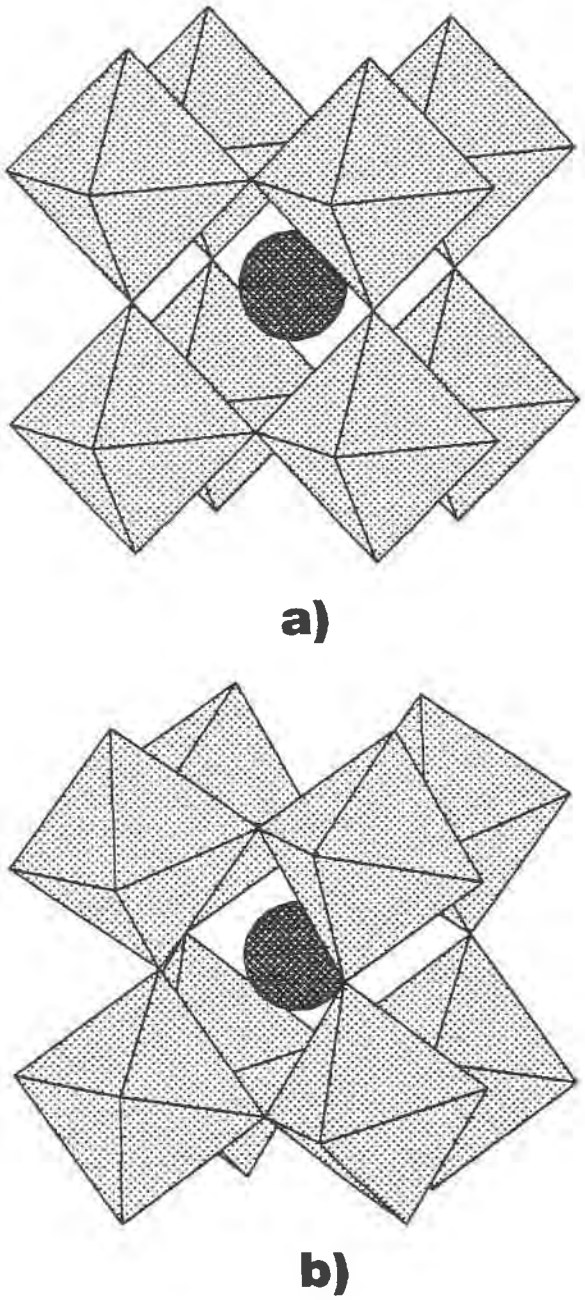

Fig. 5. $MgSiO_3$ perovskite structures. (**a**) Ideal cubic structure (*Pm*3*m*); (**b**) distorted orthorhombic structure (*Pbnm*). Octahedra contain Si, filled circles are Mg.

rotations of octahedra that reduce the effective coordination of the A cations. From powder X-ray diffraction, Yagi et al. (1978) determined that synthetic $MgSiO_3$ perovskite has an orthorhombic structure (Fig. 5b) at room temperature and pressure. Hemley et al. (1987) have carried out SSMEG calculations on both the ideal and the distorted structures of $MgSiO_3$ and $CaSiO_3$ over a range of volumes. Figure 6 shows that at all volumes the dis-

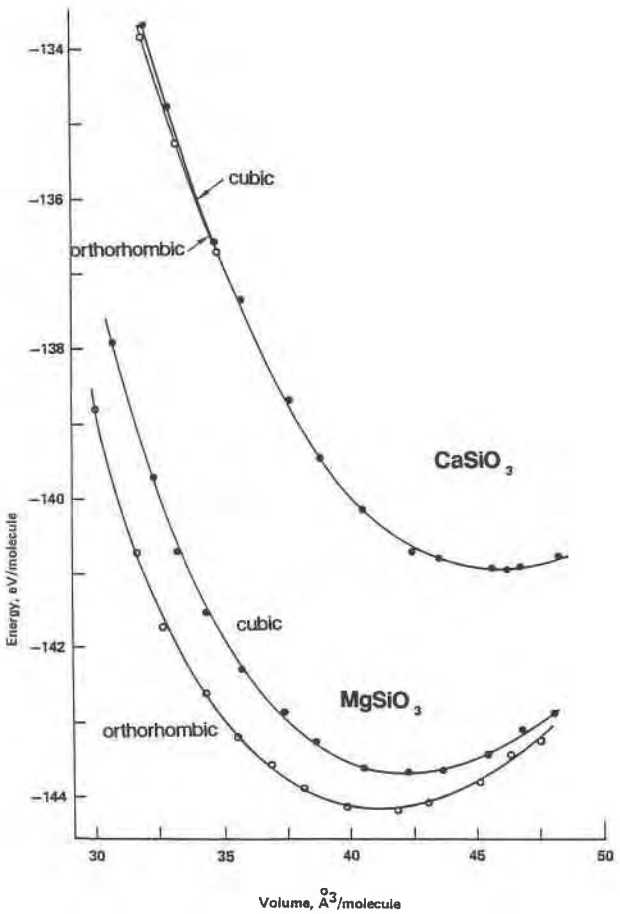

Fig. 6. SSMEG structure energy versus volume for cubic and orthorhombic structures of $MgSiO_3$ and $CaSiO_3$ perovskites. From Hemley et al. (1987).

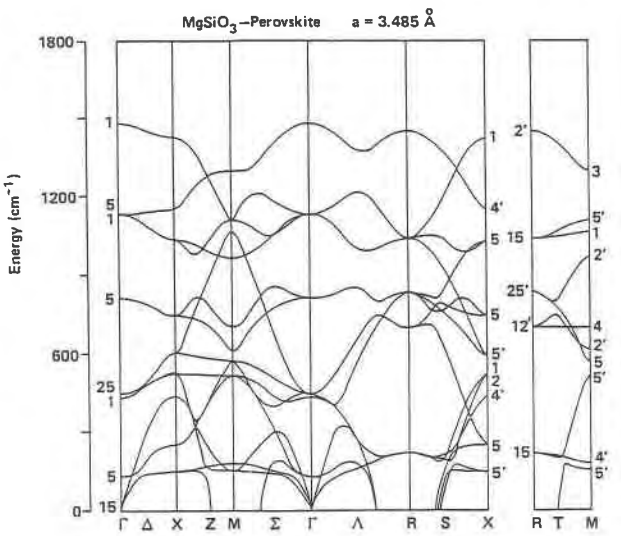

Fig. 7. Calculated phonon dispersion (vibration energy, $\propto$ to ω^2, versus wave vector) for normal vibration modes of minimum-energy cubic $MgSiO_3$ at zero pressure. Labeling of wave vector paths and points in the first Brillouin zone along the abscissa follows the Bouckaert et al. (1936) convention; mode symmetry designations were identified by comparing calculated eigenvectors with those published by Cowley (1964). From Hemley et al. (1987).

torted orthorhombic (*Pbnm*) structure for $MgSiO_3$ is more stable than the ideal cubic (*Pm*3*m*) one, whereas for $CaSiO_3$ the cubic structure is stable with respect to distortions down to about 35 Å^3/(formula unit), corresponding to a pressure of about 109 GPa (298 K). This relative stability difference clearly arises from the size difference between Mg^{2+} and Ca^{2+}.

Using the SSMEG models Hemley et al. (1987) have carried out quasiharmonic lattice dynamics calculations on both perovskite structures at different volumes. In the cubic $MgSiO_3$ structure the calculated phonon-dispersion relations (Fig. 7) show that several normal vibration modes have negative energies, hence imaginary frequencies, near the R and M points at the edge of the first Brillouin zone. The eigenvectors of these unstable modes indicate motions that correspond to librations of Si octahedra with respect to each other, thus demonstrating the dynamical instability of the ideal structure with respect to distortions arising from octahedral rotations. Phonon-dispersion relations for $CaSiO_3$ show that the corresponding modes have real frequencies at large volumes, that reduce to zero frequency at the point where the distorted orthorhombic structure becomes more stable. The distortional symmetry-reducing transformation thus takes place in response to the onset of dynamical instability with increasing pressure.

Figure 8 compares pressure-volume equations of state for orthorhombic $MgSiO_3$ calculated using three MEG variations with recent experimental data (Knittle and Jeanloz, 1987). The PIB model (Cohen, 1987) agrees very well, the SSMEG results (Hemley et al., 1987) slightly less well, and the rigid-ion MEG results (Wolf and Bukowinski, 1987) substantially less well, indicating again that it is essential to account for the effects of crystal fields on anion charge densities.

There has been some discussion regarding the variation of distortion in $MgSiO_3$ perovskite with increasing pressure. Yagi et al. (1978) predicted that the distortion from cubic symmetry would decrease with pressure, whereas O'Keeffe et al. (1979) predicted an increase. Analysis of the SSMEG model structures calculated by Hemley et al. (1987) shows that the distortion parameter Φ ($=\cos^{-1}(2^{1/2}a^2/bc)$ for the *Pbnm* orientation), which O'Keeffe et al. (1979) derive as the departure of regular octahedra from cubic orientation, ranges between 13.7° and 14.9° for structures at 0 GPa through 156 GPa, then increases to 19° for the structure at 237 GPa. Si octahedral angle variance rises fairly regularly from 0.76 for the structure at 0 GPa to 1.33 for the structure at 237 GPa, indicating a slight increase in distortion over this pressure range. The

behavior of Mg coordination is more difficult to describe: The range of all 12 Mg-O distances, Δ_{12} = Mg-O_{max} − Mg-O_{min}, increases from 0.84 Å for the structure at 0 GPa to 0.98 Å for the structure at 237 GPa, but the range for the shortest six Mg-O distances, Δ_6, remains essentially constant, and that for eight, Δ_8, decreases slightly from 0.40 Å to 0.37 Å. If one considers Mg to be eight-coordinated, which is reasonable in light of the jump of 0.2–0.4 Å (depending on pressure) between the eighth and ninth shortest Mg-O distances, the coordination polyhedron appears not to become significantly more distorted with increasing pressure; the distortion of the entire cavity, considering 12 Mg-O distances, clearly does, however. Wall et al. (1986) report inconclusive results using a variety of empirical short-range potentials determined by fittings to the experimental perovskite structure at 0 GPa (Yagi et al., 1982). One set of potentials yields model structures for which Φ remains roughly constant with pressure, whereas two other sets yield structures exhibiting a decrease of Φ with increasing pressure, in disagreement with the MEG results. The previously discussed calculated lattice dynamical behavior (Hemley et al., 1987) is consistent with distortions that increase, rather than decrease, with increasing pressure. Nevertheless, all modeling results strongly imply that the stable $MgSiO_3$ perovskite under lower mantle conditions is orthorhombic, although the degree of distortion may be similar to that of the zero-pressure structure.

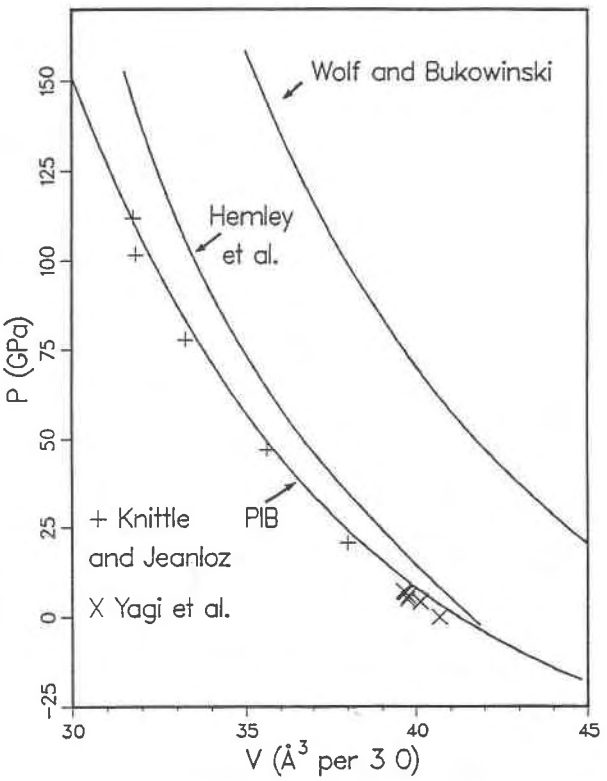

Fig. 8. Pressure-volume relations for orthorhombic $MgSiO_3$ perovskite. Calculated equations of state: PIB (Cohen, 1987); SSMEG (Hemley et al., 1987); rigid ion MEG (Wolf and Bukowinski, 1987). Experimental data from Knittle and Jeanloz (1987) and Yagi et al. (1982). From Cohen (1987).

Forsterite and Mg_2SiO_4 polymorphism

Forsterite has been modeled by a number of workers using a variety of strategies with both empirically determined and MEG-derived short-range potentials. Table 4 compares several model structures with the observed structure. The two SSMEG models (Table 4, columns 4 and 5) differ somewhat in the way minimizations were carried out, yet both have polyhedral distortions similar in character to those observed. Therefore it is fair to say that those distortions are an inherent feature of the olivine structure and do not arise from subtleties of bond character. Whereas the Jackson and Gordon (1988a) model reproduces observed distances and cell dimensions less well than the Post and Burnham (1986a) model, it better matches the observed bulk modulus; thus it is likely to be a better predictor of structural changes with pressure and of elastic properties.

The Gilbert + Morse empirical potentials (Table 4, column 2) were derived by fitting to the forsterite structure and include charge variation (Price and Parker, 1984). The fitted potential, with a Morse term for Si-O, has charges of +1.73 for Mg and −1.21 for O; the Si charge was fixed at +1.38 to preserve electrical neutrality. These can be compared with observed residual charges for forsterite of +1.75 for Mg and −1.40 for O (Fujino et al., 1981).

More recently Price et al. (1987a, 1987b) have used empirically determined potentials, labeled THB1, to carry out extensive calculations of forsterite lattice dynamical and thermodynamic properties. The Mg-O potential, described in the Born-Mayer form, was determined by fitting to periclase (Lewis, 1985). The O-O interaction was described in the Buckingham form (Eq. 22) (Catlow, 1977). The Si-O interaction was described in the Buckingham form with additional terms for O-Si-O bond bending and a further shell model to describe the polarizability of oxygen; these were determined by fitting to the structure and elastic parameters of quartz (Sanders et al., 1984). This THB1 potential tests the transferability of empirical potentials, in this case from periclase and quartz to forsterite and its β-spinel (beta-phase, wadsleyite) and γ-spinel (true spinel, ringwoodite) polymorphs. Results listed in column 3 of Table 4 demonstrate that the forsterite structure and bulk modulus are modeled better by this potential than any other at the present time.

The density-of-states histogram for forsterite (Fig. 9) was constructed by calculating vibration frequencies for 84 normal modes on a grid of 27 equally spaced points in the irreducible portion of the first Brillouin zone (Price et al., 1987b). An important feature of the vibrational characteristics of forsterite, reproduced by the lattice dynamics calculations, is the 100 cm^{-1} wide gap separating

Table 4. Comparison of observed and minimum-energy forsterite structures

		Empirical short-range potentials*		SSMEG potentials	
	Observed**	Gilbert + Morse†	Mixed THB1‡	Born-Mayer form§	"Compiled" IC‖
Unit cell					
a (Å)	4.7535(4)	4.643 (−2.3)	4.791 (+0.8)	4.874 (+2.5)	4.927 (+3.6)
b	10.1943(5)	10.416 (+2.2)	10.29 (+0.9)	10.322 (+1.2)	10.330 (+1.3)
c	5.9807(4)	6.124 (+2.4)	5.983 (+0.0)	5.977 (−0.1)	6.181 (+3.3)
V (Å³)	289.80(5)	296.17 (+2.2)	294.96 (+1.8)	300.55 (+3.7)	314.59 (+8.6)
Si Tetrahedron					
Si-O1 (Å)	1.615(3)	1.608 (−0.4)	1.622 (+0.4)	1.560 (−3.4)	1.571 (−6.1)
Si-O2	1.640(3)	1.645 (+0.3)	1.641 (+0.1)	1.606 (−2.1)	1.549 (−5.5)
Si-O3 (×2)	1.633(2)	1.634 (+0.1)	1.638 (+0.3)	1.586 (−2.9)	1.521 (−6.9)
⟨Si-O⟩	1.630	1.629 (−0.1)	1.635 (+0.3)	1.585 (−2.8)	1.527 (−6.3)
M1 Octahedron					
Mg1-O1 (×2) (Å)	2.083(2)	2.079 (−0.2)	2.051 (−1.5)	2.076 (−0.3)	2.137 (+2.6)
Mg1-O2 (×2)	2.074(2)	2.087 (+0.2)	2.097 (+1.1)	2.119 (+2.2)	2.188 (+5.5)
Mg1-O3 (×2)	2.145(3)	2.135 (−0.5)	2.209 (+3.0)	2.251 (+4.9)	2.360 (+10)
⟨Mg1-O⟩	2.101	2.100 (−0.1)	2.119 (+0.9)	2.149 (+2.3)	2.228 (+6.0)
M2 Octahedron					
Mg2-O1 (Å)	2.166(3)	2.214 (+2.2)	2.217 (+2.4)	2.332 (+7.7)	2.358 (+8.9)
Mg2-O2	2.045(5)	2.065 (+1.0)	2.026 (−0.9)	2.085 (+2.0)	2.132 (+4.3)
Mg2-O3 (×2)	2.064(4)	2.105 (+2.0)	2.038 (−1.3)	2.035 (−1.4)	2.062 (−0.1)
Mg2-O3′ (×2)	2.208(4)	2.239 (+1.4)	2.273 (+2.9)	2.353 (+6.6)	2.474 (+12)
⟨Mg2-O⟩	2.126	2.161 (+1.7)	2.144 (+0.8)	2.199 (+3.4)	2.260 (+6.3)
O2-O3 (sh)	2.558(5)	2.539 (−0.7)	2.523 (−1.4)	2.604 (+1.8)	2.334 (−8.8)
K (GPa)	140	150	154	(188)‖	144

* Numbers in parentheses are % deviations from observed values.
** Hazen (1976b); esd's are in parentheses.
† Price and Parker (1984); Morse potential for Si-O; charges varied.
‡ Price et al. (1987b); Born type for Mg-O, Buckingham type for Si-O and O-O, shell model for O, bond bending term for O-Si-O; room temperature structure.
§ Post and Burnham (1986a); O^{2-} shell radii are: O1 = 1.03 Å, O2 = 1.05 Å, O3 = 1.08 Å.
‖ Jackson and Gordon (1988a); anion self-energy included in minimization.

higher frequency modes involving internal vibrations of the SiO_4 tetrahedra from the lower frequency "lattice" modes; Kieffer (1985) has pointed out how important this feature in the density-of-states function is for proper calculation of thermodynamic properties. This calculated density-of-states function compares favorably with one determined experimentally by inelastic neutron scattering (Rao et al., 1987). Figure 10 (Price et al. (1987b) is a plot of the heat capacity, C_v, as a function of temperature calculated using Equation 17 and the density-of-states function, $G(\omega)\,d\omega$, shown in Figure 9; both that density-of-states function and a cruder one obtained using only eight sampling points in the Brillouin zone reproduce the experimentally observed heat capacity almost exactly. However, note that when frequencies are obtained only at the origin of the Brillouin zone, with one grid point corresponding to zero-wave vector, such as would be obtained from analysis of infrared- and Raman-active modes, divergence of the calculated heat capacity from the observed increases with increasing temperature.

To obtain the constant-pressure heat capacity C_p and entropy using Equations 18 and 19, the thermal Grüneisen parameter, γ_{th}, must be obtained. This is assumed equal to the average mode Grüneisen parameter, $\bar{\gamma}$, given by Equation 20. Since frequencies are related to the second derivatives of interionic potentials, it is clear that Grüneisen parameters are related to their third derivatives. Comparison of $\bar{\gamma}$, calculated using the THB1 potentials (Price et al., 1987b) with that determined experimentally (White et al., 1985; Figure 11), shows discrepancies undoubtedly related to limitations of the quasiharmonic approximation at higher temperatures. Furthermore, Price et al. (1987b) point out that the THB1 Si-O potentials yield mode γ's for Si-O stretching that are too low, perhaps by factors of 2 to 3, in spite of the fact that the frequencies themselves are well modeled (Price et al., 1987a). The calculated coefficient of volume expansion, β, matches the observed value well to 100 K through an increase of two orders of magnitude. Above that temperature the errors in the calculated Grüneisen parameters propagate to yield values for β that are low by about 35% at 1000 K (Price et al., 1987b). Nevertheless, calculated values for C_p and S agree wtih observed ones to better than 1% at 100 K and 3.5% (for C_p) and 1.2% (for S) at 1000 K.

One of the important long-term objectives of ionic modeling is to develop the ability to predict stability relations. Price et al. (1987b) have used their empirical THB1 potential to carry out calculations, similar to those just reviewed, on the wadsleyite and ringwoodite polymorphs of forsterite. In general the calculations yield values for thermodynamic properties in agreement with observation to approximately the same extent as for forsterite. Consequently the calculated $\Delta S_{1000\,K}$ values for forsterite-wadsleyite, wadsleyite-ringwoodite, and forsterite-ringwoodite agree rather well with petrologically and calorimetrically determined values; Clausius-Clapeyron slopes ($\Delta S/\Delta V$) calculated for 1000 K and 14 GPa (using calculated values for V at $P = 0$, $T = 0$, β, and K, together with an estimated value of 4 for K' (Price et al.,

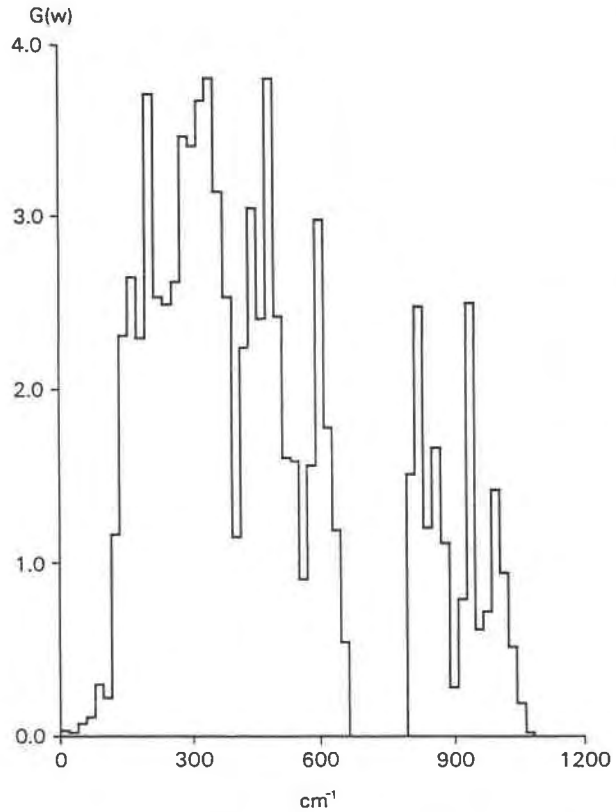

Fig. 9. Density-of-states histogram for forsterite; calculated from normal-mode frequencies sampled on a 27-point grid in the first Brillouin zone. From Price et al. (1987b).

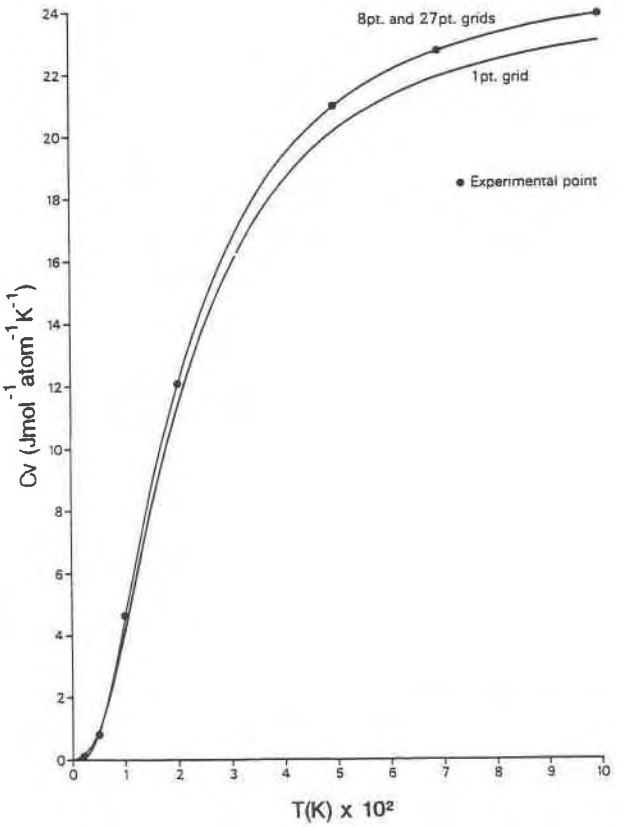

Fig. 10. Forsterite heat capacity, C_V, calculated using potential THB1. Experimental points from Robie et al. (1982) and Berman and Brown (1985). From Price et al. (1987b).

1987b)) are close to previously reported values for wadsleyite-ringwoodite but slightly lower than those for forsterite-wadsleyite and forsterite-ringwoodite.

Price et al. (1987b) took an additional step toward a predicted phase diagram for the Mg_2SiO_4 polymorphs by calculating Gibbs free energies as functions of pressure at 0 K for the three phases. They predict the forsterite → wadsleyite transition at 3.5 GPa, several GPa too low, and the wadsleyite → ringwoodite transition at 15.5 GPa, probably about 7 GPa too high. It is well known that curves of Gibbs free energy versus pressure for polymorphs with similar structures intersect at shallow angles, and thus that the pressure of intersection is strongly sensitive to very slight errors in energy. Price et al. (1987b) point out that just a 0.1% reduction in the calculated structure energy of wadsleyite will remove these pressure errors almost completely; they further suggest that such error is likely because the Si_2O_7 groups in wadsleyite make that structure relatively more difficult to model than the others. Under the assumption of constant Clausius-Clapeyron slopes, phase boundaries for these transitions are plotted in Figure 12, where they are compared with other phase boundaries estimated from experiment.

It is worth reiterating that these calculations on the structures and properties of forsterite and its polymorphs are based on interionic potentials derived from periclase and quartz, and that they were carried out under the assumptions of a pairwise additive ionic model behaving dynamically in a quasiharmonic fashion. Whereas they illustrate well the present capabilities of modeling for simulating important thermodynamic properties, they also demonstrate the need for more highly accurate interionic potentials.

Quartz

Because of the nature of Si-O bonds, well known to have significant covalent character (e.g., Gibbs, 1982), one might properly anticipate that a purely ionic model would not be appropriate for their modeling. We have already seen the introduction of empirical bond-bending terms and shell models in attempts to account for what are generally termed nonionic effects, or anisotropic anion polarizations. The tetrahedral silica frameworks are thus severe tests of the ionic model, and straightforward MEG procedures (Tossell, 1980; Post and Burnham, 1986a) fail to model quartz correctly. As column 3 of Table 5 indicates, the two distinct tetrahedral distances are simulated to be equal incorrectly, and the Si-O-Si angle is too straight by 18°. The model structure resembles high quartz more closely than it does low quartz.

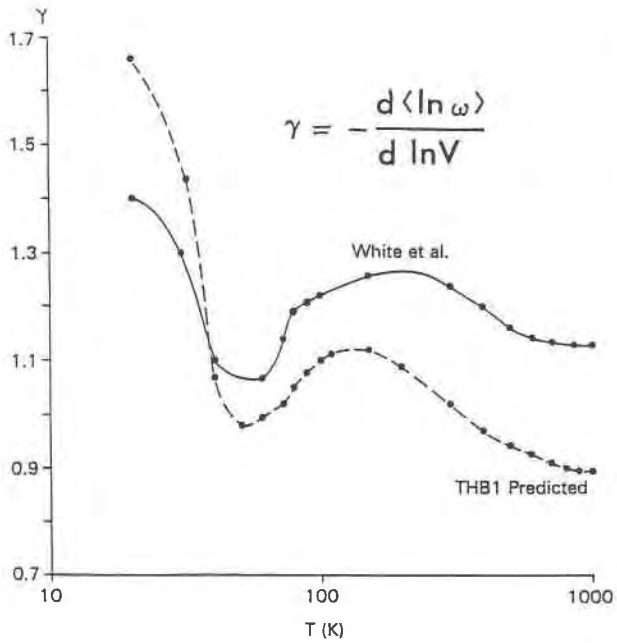

Fig. 11. Predicted and observed mean Grüneisen parameters for forsterite as a function of temperature. Calculated values based on THB1 interionic potential (Price et al., 1987b); experimental data from White et al. (1985). From Price et al. (1987b).

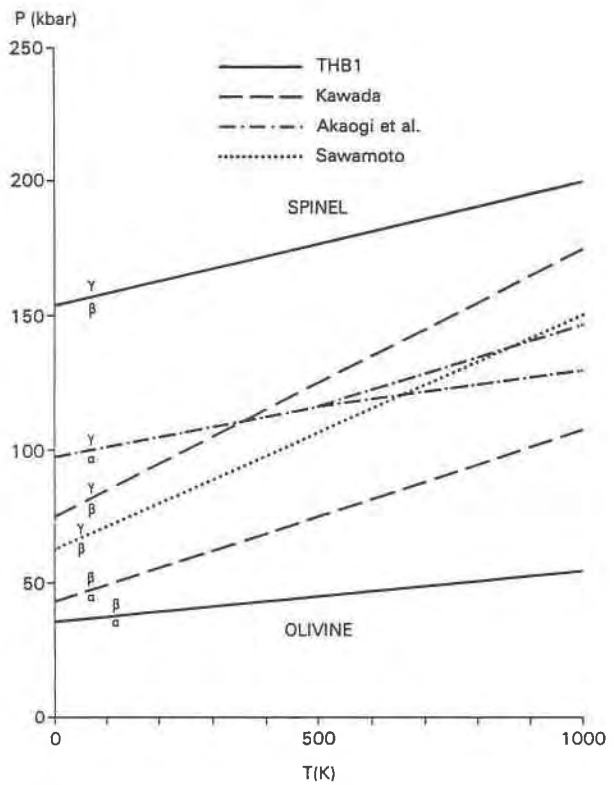

Fig. 12. Calculated and estimated phase boundaries in the Mg_2SiO_4 system. Calculated phase boundaries (solid lines) are based on THB1 interionic potentials (Price et al. (1987b)); estimates from experimental data are from Akaogi et al. (1984) (dot-dash lines), Kawada (1977) (dashed lines), and Sawamoto (1986) (dotted line). From Price et al. (1987b).

A first attempt to include anisotropic polarization in the MEG formalism has been made by Jackson and Gordon (1988b). They separate the O ion in quartz into a core with +6 charge and two shells each having charge −4. During minimization, the shells may move with respect to the core, subject to the constraint that the shell centers remain in the plane defined by the core and the two closest Si^{4+} ions. An internal shell-core potential is defined in terms of the O^{2-} dipole polarizability, and the associated shell-shell potential is defined from estimates of quadrupolar polarizability. Interionic short-range potentials for Si^{4+}-O^{2-}_{shell}, O^{2-}_{core}-O^{2-}_{shell}, and O^{2-}_{shell}-O^{2-}_{shell} were compiled by MEG methods. By allowing the O electron density to polarize anisotropically in this admittedly ad hoc manner, the quartz structure is modeled quite well

Table 5. MEG-based minimum energy structures of quartz

	Observed		MEG models	
	Low quartz*	High quartz*	Shell stabilized r_{sh} = 0.93 Å**	Two-shell polarization†
Unit cell				
a (Å)	4.91	5.01	4.97	4.85
c	5.40	5.47	5.52	5.32
V (Å³)	112.74	118.90	118.00	108.4
Interatomic distances				
Si-O (Å)	1.594	1.609	1.564	1.595
Si-O′	1.613	1.609	1.564	1.614
⟨O-O⟩	2.618	2.626	2.553	2.620
O-Si-O angles				
Range (°)	108.6–111.4	103.0–114.7	104.4–116.3	107.5–110.6
Variance (°)	1.4	28.6	29.3	1.5
Si-O-Si (°)	144.6	148.7	162.6	140.1

* Megaw (1973, pp. 263–265).
** Post and Burnham (1986a).
† Jackson and Gordon (1988b); Si-O distances are to oxygen cores; oxygen-core–shell = 0.15 Å, shell–shell = 0.28 Å, shell–core–shell = 141.4°; charges: core +6, shells −4 each.

Table 6. Observed and minimum-energy diopside structures

	Observed*	Chain stretching variable charge**	SSMEG repulsions†	SSMEG split shell model‡	Mixed THB1 and MEG‖
Unit cell					
a (Å)	9.75	9.60 (−1.5)	11.34 (+16)	10.05 (+3.1)	9.58 (−1.7)
b	8.90	9.43 (+6.0)	11.00 (+24)	9.23 (+3.7)	8.64 (−2.9)
c	5.25	5.28 (+0.6)	5.41 (+3.0)	5.20 (−0.9)	5.14 (−2.1)
β (°)	105.6	106.2 (+0.6)	118.7 (+12)	106.5 (+0.8)	104.0 (−1.5)
V (Å^3)	438.6	458.2 (+4.5)	592.3 (+35)	462.4 (+5.4)	412.5 (−6.0)
Si Tetrahedron					
Si-O1(C1) (Å)	1.60	(1.60)	1.60 (+0)	1.59 (−0.6)	1.59 (−0.6)
Si-O2(C1)	1.59	(1.59)	1.60 (+0.6)	1.59 (+0)	1.57 (−1.3)
Si-O3(C1)	1.66	1.68 (+1.2)	1.58 (−4.8)	1.62 (−2.4)	1.68 (+1.2)
Si-O3(C2)	1.69	1.67 (−1.2)	1.59 (−5.9)	1.63 (−3.6)	1.70 (+0.6)
⟨Si-O⟩	1.63	1.63 (+0)	1.59 (−2.5)	1.61 (−1.2)	1.64 (+0.6)
Chain angle:					
O3C1-O3C2-O3C1′	166.4°	§	179.5° (+7.9)	157.3° (−5.5)	166.6° (+0.1)
Mg (M1) polyhedron					
Mg-O1(A1,B1) (Å)	2.12	2.24 (+5.7)	4.87 (+130)	2.32 (+9.4)	2.11 (−0.5)
Mg-O1(A2,B2)	2.06	2.02 (−1.9)	1.96 (−4.9)	2.06 (+0)	2.05 (−0.5)
Mg-O2(C1,D1)	2.05	2.09 (+2.0)	1.96 (−4.4)	2.17 (+5.9)	1.99 (−2.9)
⟨Mg-O⟩	2.08	2.12 (+3.4)	§§	2.18 (+4.8)	2.05 (−1.4)
Mg-Mg	3.10	3.23 (+4.2)	4.98 (+60)	3.19 (+2.9)	3.03 (−2.3)
Ca (M2) polyhedron					
Ca-O1(A1,B1) (Å)	2.36	2.43 (+3.0)	2.16 (−8.5)	2.25 (−4.7)	2.26 (−4.2)
Ca-O2(C2,D2)	2.35	2.32 (−1.3)	2.16 (−8.1)	2.22 (−5.5)	2.32 (−1.3)
Ca-O3(C1,D1)	2.56	2.70 (+5.5)	3.72 (+45)	2.92 (+14)	2.45 (−4.3)
Ca-O3(C2,D2)	2.72	2.77 (+1.8)	4.50 (+65)	3.06 (+12)	2.57 (−5.5)
⟨Ca-O⟩	2.50	2.55 (+2.0)	§§	2.61 (+4.4)	2.39 (−4.4)

Note: Numbers in parentheses are % deviations from observed values.

* Cameron et al. (1973); atom notation from Burnham et al. (1967).

** Matsui and Busing (1984); Gilbert-type potentials with variable charges; $q_{Mg,Ca}$ fixed at +2.0, $q_{O1,O2}$ fitted at −1.26, q_{O3} fitted at 0.905, q_{Si} set to +1.425 to maintain neutrality; see reference for other potential parameters.

† Post and Burnham (1986a); O^{2-} shell radii: O1, 2 = 1.11 Å; O3 = 0.93 Å.

‡ Abbott (unpublished); split shells on O3 with quartz configuration (Jackson and Gordon, 1988b).

‖ Dove (1989); THB1 Mg-O and Si-O potentials (Price et al., 1987a); MEG potential for Ca-O (Post and Burnham, 1986a).

§ Value not available.

§§ Value of no significance.

(Table 5, column 4). The minimum-energy configuration places the centers of the O shells 0.15 Å away from the core, approximately along the Si-O_{core} vectors, with a shell-shell distance of 0.28 Å and a shell-core-shell angle of 141.4°, compared with the Si-O_{core}-Si angle of 140.1°. The model correctly simulates unequal Si-O distances and softens the structure appropriately to yield a calculated bulk modulus (55 GPa) too large by a factor of only 1.5, instead of the factor of about 8 (300 GPa) derived from the unpolarized SSMEG model (Jackson and Gordon, 1988b). This split-shell model for O improves the simulation of low cristobalite to a similar degree (Jackson and Gordon, 1988b). Although it lacks the theoretical foundation embodied in MEG formalisms, this exploratory treatment of anions exposed to asymmetric potential gradients that occur in many low-symmetry low-coordination environments merits further serious development based on its initial successes.

Diopside

This prototypical single silicate chain structure stands as a strong challenge to the ionic model because, in addition to its monoclinic symmetry, the Si tetrahedra and eight-coordinated Ca polyhedra are significantly distorted, and, more importantly, all three O atoms in its asymmetric unit lack Pauling local electrostatic charge balance. The chain-linking O atoms, O3, bonded to two adjacent Si ions plus two Ca ions, have bond-strength sums of 2.5, whereas O1, coordinated by one Si, two six-coordinated Mg and one Ca, has a bond-strength sum of 1.9, and O2, coordinated by one Si, one Mg, and one Ca, has a bond strength sum of only 1.6. The consequences of these local charge imbalances to bond distances and polyhedral distortions are well documented (e.g., Cameron et al., 1973).

Matsui and Busing (1984) developed an empirical model for diopside (Table 6, column 2) that reproduced elastic constants reasonably well, with maximum and minimum deviations from observation of 57% and 3%, and a mean deviation of only 18%. Their model simulated the silicate chain in terms of bond-bending potential terms for Si-O-Si and O-Si-O angles and a bond-stretching term for Si-O3; Si-O1 and Si-O2 distances were not varied. Charges on O1 (=O2) and O3 were varied, the Si charge was adjusted (to +1.425) to preserve neutrality, and Mg and Ca charges were fixed at +2. Empirically determined Gilbert-type repulsion terms (Eq. 21) were used for Mg-O and Ca-O.

Post and Burnham (1986a) showed that SSMEG procedures fail to reproduce the diopside structure but, curiously, yield a different structure having a straight silicate chain, Si tetrahedra with distortions opposite of those observed (short instead of long Si-O3 distances), and four-

coordinated Mg and Ca ions (Table 6, column 3); this incorrect structure exhibits, however, total local electrostatic charge balance on all oxygens. We suggested that the purely ionic MEG pair potentials simulate the structure diopside would assume if it were completely ionic and that the observed departures from this model structure arise from nonionic bonding effects.

Abbott (personal communication) has cleverly demonstrated that if anisotropic polarization effects on the chain-linking O3 are taken into account, a substantially improved structure can be simulated by SSMEG methods (Table 6, column 4). He modeled O3 with a fixed split-shell configuration taken from that determined by Jackson and Gordon (1988b) for low quartz. The shell-core-shell arrangement, whose details are given above, was permitted to rotate and translate as a rigid body in the diopside minimization. The resulting structure has the correct coordinations, qualitatively correct polyhedral distortions, and a reasonable silicate chain, slightly more bent than the observed one. The success of this procedure suggests that what may be nonionic bonding effects can be effectively treated within the ionic modeling framework as anisotropic polarizations.

Very recently Dove (1989) reported an excellent simulation of the diopside structure using the same THB1 empirical potentials for Mg-O, Si-O, and O-O that Price et al. (1987a, 1987b) applied so successfully to Mg_2SiO_4 polymorphs, combined with the MEG-determined Ca-O potentials given by Post and Burnham (1986a). His model structure (Table 6, column 5) reproduces the observed chain configuration and all polyhedral distortions quite well, further extending the apparent transferability of periclase-fitted Mg-O and quartz-fitted Si-O pair potentials. Elastic moduli calculated with these potentials match observed values less well than those of Matsui and Busing (1984), with maximum, minimum, and mean deviations of 114%, 3%, and 35%, respectively. However, this model permitted complete structure adjustment, which the Matsui and Busing (1984) model, specifically designed to reproduce elastic moduli, did not.

I anticipate that in the near future a variety of interesting pyroxene crystal-chemical problems will be pursued using modeling now that both empirical and MEG strategies for obtaining pair potentials show promise. It is abundantly clear, however, that future success following the nonempirical MEG avenue hinges on suitable handling of anisotropic anion polarizations. The empirical route requires suitably transferable potentials for a number of cation-anion pairs beyond Mg-O and Si-O to begin to range over the wide compositional realm of pyroxenes; whether these can be obtained has yet to be determined.

Albite

In my final example, I want to illustrate how ionic static structure-energy calculations on a complex low-symmetry structure can provide substantial insights on crystal chemical behavior related to order-disorder phenomena.

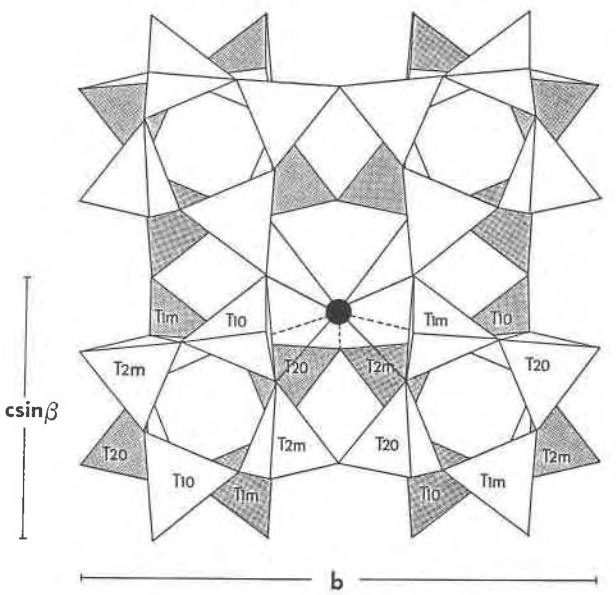

Fig. 13. Projection of the monoclinic ($C2/m$) albite structure down **a**, showing four crystallographically distinct T sites and the nine-coordinated Na atom (solid circle). From Post and Burnham (1987).

Ordered low albite. Full energy minimizations on the ordered triclinic low-albite structure, carried out by Post and Burnham (1987) using SSMEG short-range potentials, confirm that the driving force for Al ordering into the $T_1$0 tetrahedral sites (see Fig. 13) is provided by the triclinic lattice distortions. Separate energy minimizations on the low-albite structure with Al ordered in turn into each of the crystallographically distinct T sites led to unit cells and energies given in Table 7. Since, apart from chemical occupancy, $T_1$0 and T_1m are equivalent in the monoclinic structure, as are $T_2$0 and T_2m, we would anticipate that, as atomic coordinates and lattice parameters relax, the triclinic minimum-energy structures with Al in $T_1$0 and T_1m would be related as are albite twins, by reflection through the monoclinic (010). Relaxed structures with Al in $T_2$0 and T_2m ought to be related similarly. The cell parameters in Table 7 show such relationships, more precisely for $T_1$0 and T_1m structures than for $T_2$0 and T_2m. Likewise the relative energies of twin-related ordered structures ought to be the same, as Table 7 shows they are exactly for $T_1$0 and T_1m, and nearly so for $T_2$0 and T_2m. The relative energies for T_1 versus T_2 differ by a rather small amount: Al is favored in T_1(0 or m) over T_2(0 or m) by only about 9.6 kJ/mol. A critical result is that the relaxed triclinic cells for Al in T_1 are more distorted from monoclinic geometry than are those for Al in T_2. When the minimizations are repeated under constraints of monoclinic lattice geometry, structures with Al in T_2 yield slightly lower energies. Thus the driving

Table 7. Low albite energy minimizations

	Aluminum in			
	$T_1$0	T_1m	$T_2$0	T_2m
Energy (kJ/anion)	−5054.8	−5054.8	−5053.5	−5053.8
Unit cell: a (Å)	8.40	8.38	8.19	8.20
b	12.98	12.98	13.30	13.24
c	7.22	7.22	7.13	7.11
α (°)	95.3	84.7	90.7	93.2
β	116.5	116.5	115.7	115.7
γ	87.4	92.6	90.5	89.6
Minimizations under monoclinic constraints ($\alpha = \gamma = 90°$):				
Energy (kJ/anion)	−5052.8	−5054.0	−5054.5	−5054.5

force for Al to order into $T_1$0 (or T_1m) derives from the energetically favorable lattice distortions that result from that choice.

Disordered high albite and the behavior of Na. Strategies for carrying out structure-energy calculations on disordered structures are not well developed. Use of average charges for sites with disordered occupancies by cations with different valences is known to be incorrect (Giese, 1975; Jones et al., 1990), since the average pair potential is correct for neither cation-anion interaction. It would thus appear that simulation of a disordered structure requires an approximation made as some kind of average of many different ordered states, even including some with reduced symmetry and supercells. Jones et al. (1990) suggest, however, that judicious splitting of sites may permit direct simulation of structures containing disordered cation occupancies in polyhedra whose anions take up different positions depending on specific local cation species.

To examine the response of Na atoms to different local tetrahedral Al/Si cation distributions in the high-albite framework, Post and Burnham (1987) carried out partial structure-energy minimizations using fixed observed frameworks (tetrahedral cation and oxygen positions) with a variety of specific local Al/Si distributions, and varied the positions of the Na atoms. Taking observed framework atom positions from structure analyses of high albite at room temperature and 1090 °C (Prewitt et al., 1976), we calculated structure energies and Na positions for the 55 arrangements of 4 Al and 12 Si over 16 tetrahedral sites per unit cell that obey aluminum-avoidance (i.e., that have no two adjacent tetrahedra containing Al). These calculations demonstrated that the minimum-energy Na position is sensitive to the surrounding local tetrahedral Al/Si distribution. We further showed that the Na quarter-atoms used in high-albite structure refinements (Prewitt et al., 1976; Ribbe et al., 1969) constitute an approximation to an electron density in the feldspar cavity that is effectively a superposition of many slightly different Na positions, each of which is fixed by the particular local Al/Si distribution in the immediately surrounding tetrahedra (Post and Burnham (1987), Figs. 3 and 5).

Similar calculations on hollandite (Post and Burnham, 1986b) and on amphiboles (Docka et al., 1987) have shown a broadly demonstrable phenomenon that relatively large low-charge cations occupying sites with relatively high and somewhat ill-defined coordinations will respond to changes in distributions of cations with different valences in the surrounding tetrahedral or octahedral sites. As the local distribution of cations changes, the precise configuration of electrostatic potential also changes, thus moving the potential minimum in the cavity. The characteristically large thermal parameters and smeared electron densities exhibited by tunnel cations in some hollandites and by A-site occupants in chemically complex amphiboles are readily explained as positional variations that can be quantitatively evaluated by ionic modeling in this manner. Since the minimum-energy cavity positions are dictated by local framework cation distributions, positional "disorder" of cavity cations will not add to configurational entropy unless particular framework cation distributions yield multiple equal-energy cavity minima.

Tetrahedral site energetics versus temperature and Al/Si disordering. Our high-albite calculations provide additional insights regarding order-disorder relationships. Using the observed high-albite frameworks from six structure analyses from room temperature to 1090 °C, we calculated the energies of hypothetical ordered structures with Al in each of the four distinct sites, plotted in Figure 14. At 1090 °C the energies of structures with Al in $T_1$0 and T_1m are nearly equal as are those with Al in $T_2$0 and T_2m; this is expected, since the framework of high albite at that temperature is nearly, but not quite, monoclinic (monalbite). Al favors T_1 over T_2 by some 5 kJ/anion, or 40 kJ/mol, substantially more than in the fully minimized low-albite structures (Table 7), but this difference is likely an artifact of using the fixed frameworks in the high-albite calculations. In the room-temperature high-albite framework, Al is strongly favored in $T_1$0, even over T_1m, since the fixed framework has a particular triclinic distortion developed with decreasing temperature along a path dictated by the real disordered, but unchanging, Al/Si distribution. Finally, it is particularly instructive to note that essentially all of the energetic favorability Al achieves for concentration into $T_1$0 has been gained by framework distortions between 1090 °C and about 700 °C. This observation is entirely consistent with, and reinforces, the conclusion, reached theoretically by Salje et al. (1985) and experimentally by Goldsmith and Jenkins (1985), that most of the ordering in albite takes place over this limited temperature range.

Having calculated static structure energies for 55 Al/Si arrangements using the observed 1090 °C high-albite framework (Fig. 15), it is now possible to estimate the energy of disorder, which, neglecting the small $p\Delta V$ term, is equivalent to the static contribution to the disordering enthalpy. Assuming that the actual disordered Al/Si distribution will follow a Boltzmann distribution, the Boltzmann-weighted average energy will be (Binder, 1976):

$$\langle W \rangle = \frac{\sum W_n \exp(-W_n/kT)}{\sum \exp(-W_n/kT)} \qquad (28)$$

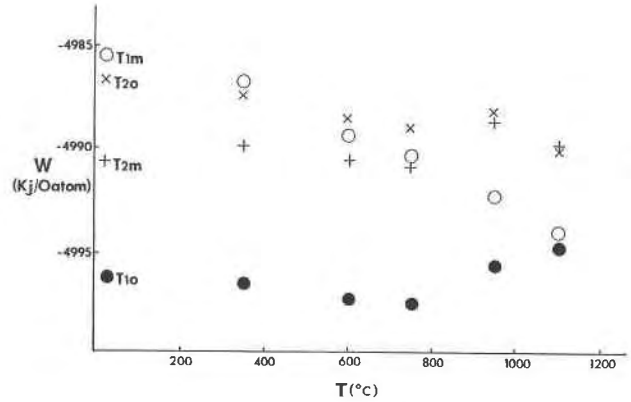

Fig. 14. High albite structure energy versus temperature. Calculations based on fixed observed tetrahedral frameworks (Prewitt et al., 1976) and minimized Na positions. Al ordered into $T_1 0$ (solid circles), $T_1 m$ (open circles), $T_2 0$ (×s), and $T_2 m$ (+s). From Post and Burnham (1987).

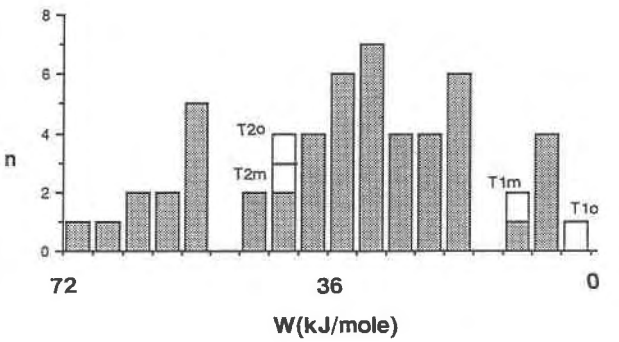

Fig. 15. Histogram of calculated structure energies for the 1090 °C high albite framework, with minimum-energy Na positions, for 55 Al/Si configurations. Configurations corresponding to Al ordered into particular crystallographic sites are indicated. Energies are relative to the lowest energy configuration, with Al in $T_1 0$.

where the summation is over all possible Al/Si distributions. Our sum is over the 55 distributions investigated, which is a small fraction of the total number, all the rest of which violate aluminum avoidance to some degree. Assuming the aluminum-avoidance principle (Loewenstein, 1954) has a valid energetic basis, which appears to be the case (e.g., Cohen and Burnham, 1985), our 55 configurations will be the most significant contributors to the Boltzmann distribution. For the 1090 °C (1363 K) high-albite framework, $\langle W \rangle$ is +12.3 kJ/mol relative to the lowest-energy ordered configuration, with Al in $T_1 0$. Thus our estimate is that $\Delta H_{o\text{-}d} \simeq 12.3$ kJ/mol at 1363 K. Carpenter et al. (1985) has determined from calorimetry that $\Delta H_{o\text{-}d} \simeq 12.6 \pm 1.3$ kJ/mol at 973 K, of which he estimated that about 1.3 kJ/mol is due to ΔC_p. Thus, the static $\Delta H_{o\text{-}d}$ at 973 K would be about +11.3 kJ/mol, to which our estimate, calculated for 1363 K with the static ionic model, compares remarkably well. At the very least it confirms that the many Al/Si configurations that violate aluminum avoidance are not significant contributors to the Boltzmann distribution.

Concluding remarks

These results demonstrate that the ionic model is quantitatively useful even for structures in which electronegativity differences indicate that the ionic character of the bonding is not high and in which residual charges on ions are known from observation to be significantly less than their formal charges. Pair potentials determined from fitting to simple structures appear to have reliable transferability into an encouragingly wide spectrum of complex structures. Theoretically determined MEG pair potentials can be used productively to simulate a variety of complex structures, and the breadth of successful structure simulations continues to grow rapidly. In sites where potential field gradients are substantial and anion electron densities are polarized, successful modeling requires that pair potentials be modified to account for these anisotropic effects. The development of improved techniques for handling anisotropic anion polarizations is imminent.

Calculation and prediction of those properties that depend on derivatives of pair potentials higher than the first are less precise and reliable. This is particularly true of elastic moduli and Grüneisen parameters, where differences between calculated and observed values of factors of two or more are not uncommon. There may, in fact, be impenetrable barriers; Hemley (personal communication) suggests, for example, that it may be impossible with MEG or other nonempirical models to simulate well both a complex structure and its elastic properties simultaneously with full formal ion charges.

Even for complex low-symmetry structures, our present ionic modeling techniques let us answer many of the "Why's" of crystal chemical behavior and let us make reasonably good structural predictions at levels of detail impossible with earlier semi-quantitative methods. Relative stabilities of polymorphs and alternative hypothetical structures can be determined with reasonable confidence. But when it comes to predicting phase changes at elevated temperatures and pressures, the results are far less reliable. Imprecision in higher derivatives of pair potentials and crudeness in handling polarization effects generate errors in properties such as thermal expansion, heat capacities, and compressibilities that have significant effects on derived equations of state and critical features of phase diagrams. I am confident that our potential models will improve, however, and that reliable calculation of phase diagrams will become a reality in the foreseeable future.

We are close to having the power of a supercomputer on our desktops and in our classrooms. We have precise structural data on an extraordinary wealth of mineral species, provided by literally thousands of structure refinements with precisely measured diffraction data over the past thirty years. These two realities ought to be powerful forces tending to alter fundamentally the way we

teach mineralogy. As overdue pedagogical transformations take place, I believe it is important to remember the value of relatively simple informative models. Sir Lawrence Bragg was especially lucid with respect to the place of such models:

> Solid bodies consist of atomic nuclei and of electrons, and the structure assumed by any solid is such that the whole system of nuclei and electrons takes up a form of minimal potential energy. The energy of a configuration is to be calculated by applying the principles of quantum mechanics and no distinction between [the] various types of [bonding] force appears in the rigid mathematical expressions. It only appears when we find it possible to get an approximation to the truth by making simplifying assumptions appropriate to the case considered. (Bragg, 1937, p. 29)

The reality is that bonding in minerals is not purely ionic. My perception is, however, that the ionic model is an approximation to the truth appropriate to the case of many complex silicates and oxides. I hope it will become the perception of others as well.

Acknowledgments

I want to thank several collaborators and my former graduate students and post-doctoral fellows for years of encouragement and stimulation. David Bish, Jeff Post, Ron Cohen, Richard Abbott, Page Chamberlain, Jan Docka, Linda Pinckney, and Mark van Baalen have all shared my enthusiasm for the potential of the ionic model to enlighten our perceptions of silicate crystal chemistry. I especially thank Yoshikazu Ohashi for pointing the way back in the early 1970s. Roy Gordon and his students Carl Muhlhausen, Mark Jackson, and Russ Hemley have generously assisted us with aspects of MEG modeling. I thank the National Science Foundation for supporting my research through grants EAR 79-20095 and EAR 87-20666. Finally I thank Jeff Post for carefully scrutinizing the manuscript on very short notice.

References cited

Akaogi, M., Ross, N.L., McMillan, P., and Navrotsky, A. (1984) The Mg_2SiO_4 polymorphs (olivine, modified spinel and spinel)—thermodynamic properties from oxide melt solution calorimetry, phase relations and models of lattice vibrations. American Mineralogist, 69, 499–512.

Berman, R.G., and Brown, T.H. (1985) Heat capacity of minerals in the system Na_2O-K_2O-CaO-MgO-FeO-Fe_2O_3-Al_2O_3-SiO_2-TiO_2-H_2O/-CO_2: Representation, estimation, and high temperature extrapolation. Contributions to Mineralogy and Petrology, 89, 168–183.

Bertaut, F. (1952) L'energie electrostatique de reseaux ioniques. Le Journal de Physique et le Radium, 13, 499–505.

Binder, K. (1976) Monte Carlo investigations of phase transitions and critical phenomena. In K. Binder, Ed., Phase transitions and critical phenomena, 5b, 1–105. Academic Press, New York.

Born, M., and Huang, K. (1954) Dynamical theory of crystal lattices. Oxford University Press, London.

Born, M., and Landé, A. (1918) Über die absolute Berechnung der Kristalleigenschaften mit Hilfe Bohrscher Atommodelle. Sitzungsberichte der Preussischen Akademie der Wissenschaften Berlin, 45, 1048–1068.

Born, M., and Mayer, J.E. (1932) Zur Gittertheorie der Ionenkristalle. Zeitschrift für Physik, 75, 1–18.

Bouckaert, L.P., Smoluchowski, R., and Wigner, E. (1936) Theory of Brillouin zones and symmetry properties of wave functions in crystals. Physical Review, 50, 58–67.

Boyer, L.L., Mehl, M.J., Feldman, J.L., Hardy, J.R., Flocken, J.W., and Fong, C.Y. (1985) Beyond the rigid ion approximation with spherically symmetric ions. Physical Review Letters, 54, 1940–1943.

Bragg, W. L. (1937) Atomic structure of minerals. Cornell University Press, Ithaca, New York.

Burnham, C.W., Clark, J.R., Papike, J.J., and Prewitt, C.T. (1967) A proposed crystallographic nomenclature for clinopyroxene structures. Zeitschrift für Kristallographie, 125, 109–119.

Burnham, C.W. (1985) Mineral structure energetics and modeling using the ionic approximation. Mineralogical Society of America Reviews in Mineralogy, 14, 347–388.

Busing, W.R. (1981) WMIN, a computer program to model molecules and crystals in terms of potential energy functions. U.S. National Technical Information Service, ORNL-5747.

Busing, W.R., and Matsui, M. (1984) The application of external forces to computational models of crystals. Acta Crystallographica, A40, 532–538.

Cameron, M., Sueno, S., Prewitt, C.T., and Papike, J.J. (1973) High-temperature crystal chemistry of acmite, diopside, hedenbergite, jadeite, spodumene, and ureyite. American Mineralogist, 58, 594–618.

Carpenter, M.A., McConnell, J.D.C., and Navrotsky, A. (1985) Enthalpies of ordering in the plagioclase feldspar solid solution. Geochimica et Cosmochimica Acta, 49, 947–966.

Catlow, C.R.A. (1977) Point defect and electronic properties of uranium dioxide. Proceedings of the Royal Society London, A353, 533–561.

Clugston, M.J. (1978) The calculation of intermolecular forces: A critical examination of the Gordon-Kim model. Advances in Physics, 27, 893–912.

Cochran, W. (1973) The dynamics of atoms in crystals. Edward Arnold, London.

Cohen, A.J., and Gordon, R.G. (1975) Theory of the lattice energy, equilibrium structure, elastic constants, and pressure-induced phase transitions in alkali-halide crystals. Physical Review, B12, 3228–3241.

Cohen, A.J., and Gordon, R.G. (1976) Modified electron gas study of the stability, elastic properties, and high pressure behavior of MgO and CaO crystals. Physical Review, B14, 4593–4605.

Cohen, R.E. (1987) Elasticity and equation of state of $MgSiO_3$ perovskite. Geophysical Research Letters, 14, 1053–1056.

Cohen, R.E., Boyer, L.L., and Mehl, M.J. (1987) Theoretical studies of charge relaxation effects on the statics and dynamics of oxides. Physics and Chemistry of Minerals, 14, 294–302.

Cohen, R.E., and Burnham, C.W. (1985) Energetics of ordering in aluminous pyroxenes. American Mineralogist, 70, 559–567.

Cowley, R.A. (1964) Lattice dynamics and phase transitions of strontium titanite. Physical Review, 134, A981.

Docka, J.A., Post, J.E., Bish, D.L., and Burnham, C.W. (1987) Positional disorder of A-site cations in $C2/m$ amphiboles: Model energy calculations and probability studies. American Mineralogist, 72, 949–958.

Dove, M.T. (1989) On the computer modeling of diopside: Toward a transferable potential for silicate minerals. American Mineralogist, 74, 774–779.

Evans, R.D. (1966) An introduction to crystal chemistry, 2nd edition. Cambridge University Press, New York.

Ewald, P.P. (1921) The calculation of optical and electrostatic lattice potentials. Annals of Physics (Leipzig), 64, 253–287.

Fujino, K., Sasaki, S., Takéuchi, Y., and Sadanaga, R. (1981) X-ray determination of electron distribution in forsterite, fayalite and tephroite. Acta Crystallographica, B37, 513–518.

Gibbs, G.V. (1982) Molecules as models for bonding in silicates. American Mineralogist, 67, 421–450.

Giese, R.F., Jr. (1975) Electrostatic energy of columbite/ixiolite. Nature, 256, 31–32.

Gilbert, T.L. (1968) Soft-sphere model for closed-shell atoms and ions. Journal of Chemical Physics, 49, 2640–2642.

Gillespie, C.C. (Editor-in-chief) (1970) Dictionary of Scientific Biography, 2, 326–332. Scribner, New York.

Goldsmith, J.R., and Jenkins, D.M. (1985) The high-low albite relations revealed by reversal of degree of order at high pressures. American Mineralogist, 70, 911–923.

Gordon, R.G., and Kim, Y.S. (1972) Theory for the forces between closed-shell atoms and molecules. Journal of Chemical Physics, 56, 3122–3133.

Hazen, R.M. (1976a) Effects of temperature and pressure on the cell dimension and X-ray temperature factors of periclase. American Mineralogist, 61, 266–271.

——— (1976b) Effects of temperature and pressure on the crystal structure of forsterite. American Mineralogist, 61, 1280–1293.
Hemley, R.J., and Gordon, R.G. (1985) Theoretical study of solid NaF and NaCl at high pressures and temperatures. Journal of Geophysical Research, 90, 7803–7813.
Hemley, R.J., Jackson, M.D., and Gordon, R.G. (1985) First-principles theory for the equations of state of minerals at high pressures and temperatures: Application to MgO. Geophysical Research Letters, 12, 247–250.
——— (1987) Theoretical study of the structure, lattice dynamics, and equations of state of perovskite-type $MgSiO_3$ and $CaSiO_3$. Physics and Chemistry of Minerals, 14, 2–12.
Jackson, M.D., and Gordon, R.G. (1988a) A MEG study of the olivine and spinel forms of Mg_2SiO_4. Physics and Chemistry of Minerals, 15, 514–520.
——— (1988b) MEG investigation of low pressure silica—Shell model for polarization. Physics and Chemistry of Minerals, 16, 212–220.
Jeanloz, R., and Thompson, A.B. (1983) Phase transitions and mantle discontinuities. Reviews of Geophysics and Space Physics, 21, 51–74.
Jones, I.L., Heine, V., Leslie, M., and Price, G.D. (1990) A new approach to simulating disorder in crystals. Physics and Chemistry of Minerals, in press.
Kawada, K. (1977) The system Mg_2SiO_4-Fe_2SiO_4 at high pressures and temperatures and the Earth's interior. Ph.D. thesis, University of Tokyo.
Kieffer, S.W. (1985) Heat capacity and entropy: Systematic relations to lattice vibrations. Mineralogical Society of America Reviews in Mineralogy, 14, 65–126.
Knittle, E., and Jeanloz, R. (1987) Synthesis and equation of state of $(Mg,Fe)SiO_3$ perovskite to over 100 gigapascals. Science, 235, 668–670.
Lasaga, A.C. (1980) Defect calculations in silicates: Olivine. American Mineralogist, 65, 1237–1248.
Lewis, G.V. (1985) Interatomic potentials: Derivation of parameters for binary oxides and their use in ternary oxides. Physica, 131B, 114–118.
Loewenstein, W. (1954) The distribution of aluminum in the tetrahedra of silicates and aluminates. American Mineralogist, 39, 92–96.
Madelung, E. (1918) Das elektrische Feld in Systemen von regelmässig angeordneten. Physikalische Zeitschrift, 19, 524–532.
Matsui, M., and Busing, W.R. (1984) Calculation of the elastic constants and high-pressure properties of diopside, $CaMgSi_2O_6$. American Mineralogist, 69, 1090–1095.
McMillan, P. (1985) Vibrational spectroscopy in the mineral sciences. Mineralogical Society of America Reviews in Mineralogy, 14, 9–63.
Megaw, H.D. (1973) Crystal structures: A working approach. W. B. Saunders Co., Philadelphia.
Mehl, M.J., Hemley, R.J., and Boyer, L.L. (1986) Potential-induced breathing model for the elastic moduli and high-pressure behavior of the cubic alkaline-earth oxides. Physical Review, B33, 8685–8696.
Muhlhausen, C., and Gordon, R.G. (1981a) Electron-gas theory of ionic crystals, including many-body effects. Physical Review, B23, 900–923.
——— (1981b) Density-functional theory for the energy of crystals: Test of the ionic model. Physical Review, B24, 2147–2160.
Navrotsky, A., and Kleppa, O.J. (1967) Enthalpy of the anatase-rutile transformation. Journal of the American Ceramic Society, 50, 626.
Nijboer, B.R.A., and DeWette, F.W. (1957) On the calculation of lattice sums. Physica, 23, 309–321.
Ohashi, Y., and Burnham, C.W. (1972) Electrostatic and repulsive energies of the M1 and M2 cation sites in pyroxenes. Journal of Geophysical Research, 77, 5761–5766.
O'Keeffe, M., Hyde, B.G., and Bovin, J.-O. (1979) Contribution to the crystal chemistry of orthorhombic perovskites: $MgSiO_3$ and $NaMgF_3$. Physics and Chemistry of Minerals, 4, 299–305.
Pachalis, E., and Weiss, A. (1969) Hartree-Fock-Roothan wave functions, electron density distribution, diamagnetic susceptibility, dipole polarizability, and antishielding factor for ions in crystals. Theoretica Chimica Acta, 13, 381–408.
Parker, S.C. (1983) Prediction of mineral crystal structures. Solid State Ionics, 8, 179–186.
Pauling, L. (1927) The sizes of ions and the structure of ionic crystals. Journal of the American Chemical Society, 49, 765–790.
——— (1928) The sizes of ions and their influence on the properties of salt-like compounds. Zeitschrift für Kristallographie, 67, 377–404.
Post, J.E., and Burnham, C.W. (1986a) Ionic modeling of mineral structures and energies in the electron gas approximation: TiO_2 polymorphs, quartz, forsterite, diopside. American Mineralogist, 71, 142–150.
——— (1986b) Modeling tunnel-cation displacements in hollandites using structure-energy calculations. American Mineralogist, 71, 1178–1185.
——— (1987) Structure-energy calculations on low and high albite. American Mineralogist, 72, 507–514.
Prewitt, C.T., Sueno, S., and Papike, J.J. (1976) The crystal structures of high albite and monalbite at high temperatures. American Mineralogist, 61, 1213–1225.
Price, G.D., and Parker, S.C. (1984) Computer simulation of the structural and physical properties of the olivine and spinel polymorphs of Mg_2SiO_4. Physics and Chemistry of Minerals, 10, 209–216.
Price, G.D., Parker, S.C., and Leslie, M. (1987a) The lattice dynamics of forsterite. Mineralogical Magazine, 51, 157–170.
——— (1987b) The lattice dynamics and thermodynamics of the Mg_2SiO_4 polymorphs. Physics and Chemistry of Minerals, 15, 181–190.
Rao, K.R., Chaplot, S.L., Choudhury, N., Ghose, S., and Price, D.L. (1987) Phonon density of states and specific heat of forsterite, Mg_2SiO_4. Science, 236, 64–65.
Ribbe, P.H., Megaw, H.D., and Taylor, W.H. (1969) The albite structures. Acta Crystallographica, B25, 1503–1518.
Ringwood, A.E. (1962) Mineralogical constitution of the deep mantle. Journal of Geophysical Research, 67, 4005–4010.
Robie, R.A., Hemingway, B.S., and Takei, H. (1982) Heat capacities and entropies of Mg_2SiO_4, Mn_2SiO_4 and Co_2SiO_4 between 5 and 380 K. American Mineralogist, 67, 470–482.
Salje, E., Kuscholke, B., Wruck, B., and Kroll, H. (1985) Thermodynamics of sodium feldspar, II: Experimental results and numerical calculations. Physics and Chemistry of Minerals, 12, 99–107.
Sanders, M.J., Leslie, M., and Catlow, C.R.A. (1984) Interatomic potentials for SiO_2. Journal of the Chemical Society Chemical Communications, 1271–1273.
Sasaki, S., Fujino, K., Takéuchi, Y., and Sadanaga, R. (1980) On the estimation of atomic charges by the X-ray method for some oxides and silicates. Acta Crystallographica, A36, 904–915.
Sawamoto, H. (1986) Single crystal growth of the modified spinel and spinel phases of $(Mg,Fe)_2SiO_4$ and some geophysical implications. Physics and Chemistry of Minerals, 13, 1–10.
Sherman, J. (1932) Crystal energies of ionic compounds and thermochemical applications. Chemical Reviews, 11, 93–170.
Slater, J.C. (1939) Introduction to chemical physics. McGraw-Hill, New York.
Tossell, J.A. (1980) Calculation of bond distances and heats of formation for BeO, MgO, SiO_2, TiO_2, FeO, and ZnO using the ionic model. American Mineralogist, 65, 163–1737.
Waldman, M., and Gordon, R.G. (1979) Scaled electron gas approximation for intermolecular forces. Journal of Chemical Physics, 71, 1325–1329.
Wall, A., Price, G.D., and Parker, S.C. (1986) A computer simulation of the structure and elastic properties of $MgSiO_3$ perovskite. Mineralogical Magazine, 50, 693–707.
Watson, R.E. (1958) Analytic Hartree-Fock solutions for O^-. Physical Review, 111, 1108–1110.
White, G.K., Roberts, R.B., and Collins, J.G. (1985) Thermal properties and Gruneisen functions of forsterite, Mg_2SiO_4. High Temperatures—High Pressures, 17, 61–66.
Wolf, G.H., and Bukowinski, M.S.T. (1987) Theoretical study of the structural and thermoelastic properties of $MgSiO_3$ and $CaSiO_3$ perovskites: Implications for the lower mantle composition. In M.H. Manghnani and Y. Syono, Eds., High pressure research in mineral physics, p. 313–331. Terra Scientific, Tokyo.
Wolf, G.H., and Jeanloz, R. (1985) Lattice dynamics and structural distortions of $CaSiO_3$ and $MgSiO_3$ perovskites. Geophysics Research Letters, 12, 413–416.
Yagi, T., Mao, H.K., and Bell, P.M. (1978) Structure and crystal chemistry of perovskite-type $MgSiO_3$. Physics and Chemistry of Minerals, 3, 97–110.
Yagi, T., Mao, H.K., and Bell, P.M. (1982) Hydrostatic compression of perovskite-type $MgSiO_3$. in S.K. Saxena, Ed., Advances in Physical geochemistry, 2, 317–325. Springer-Verlag, New York.

Manuscript received January 23, 1990
Manuscript accepted March 2, 1990